Morphologies of knickpoints in submarine canyons

Neil C. Mitchell†
School of Earth, Ocean and Planetary Sciences, Cardiff University, Cardiff CF10 3YE, Wales

ABSTRACT

The question of how turbidity currents erode their beds is important for understanding how submarine canyons develop, how they maintain continuity in tectonically active margins to ensure sediment bypass, and for knowing how knickpoints (reaches of anomalously steep gradient) record tectonic information. The problem is potentially more complex than fluvial erosion, because flow vigor is also affected by the flow entraining ambient water and incorporating or depositing suspended load, which can significantly affect its excess density. However, in canyon sections where the total sedimentary mass passing through the canyon is much larger than the locally excavated mass, the solid loads of eroding currents change little during passage down-canyon. Canyon morphology can then potentially reveal how gradient and other factors affect erosion rate. Simple bed erosion models are presented herein, which are analogous to the detachment- and transport-limited erosion models of fluvial geomorphology, which predict that the channel topography should advect or diffuse (smooth out), respectively. Data sets from continental slopes off Alaska, New Jersey, Oregon, Chile, the Barbados accretionary prism, and published maps from other areas show these tendencies. Although knickpoints may arise from spatially varied resistance to erosion, some of those described here lie upstream of faults or anticlines and within uniform turbidites, implying that they can advect upstream. A forward numerical model is developed for knickpoints in the southern Barbados accretionary prism, which appear to have been created in a simple manner by the frontmost thrusts. If the erosion rules are applied continuously, the channel profiles are well represented with both advective and diffusive components. If a boundary condition of nondeposition/erosion is imposed on the base of the knickpoint slope (representing scour associated with a hydraulic jump, for example), the upstream profiles can be reproduced solely by diffusion. In these channels, the threshold stress for transport or erosion is probably small relative to stress imposed by the currents, because modeling shows that a threshold sharpens the knickpoint lip rather than rounds it. For the other, mostly smaller, knickpoints studied, however, the lip varies from sharp to rounded. This varied morphology could arise from a number of influences: effects of flow acceleration, differing threshold stress, differing sediment flux affecting flow power, or depth-varying substrate resistance to erosion. Despite the diversity of forms, upstream migrations imply that erosion can be enhanced where flow is more vigorous on steep gradients, implying that the body rather than the head of turbidity currents is responsible for erosion in those cases. Also discussed is how bed failure, quarrying, and abrasive scour lead to knickpoint evolution in submarine channels that is analogous to that in fluvial channels, but also likely differences are noted.

Keywords: accretionary prisms, tectonically active continental slopes, submarine canyon morphology, stream bed erosion.

INTRODUCTION

Since the speculations of Daly (1936), turbidity currents (in which suspended sediment is carried downslope by a turbulent flow driven by the fluid bulk density excess caused by the sediment) have been considered the submarine equivalents of rivers in carving out continental slope canyons. Just as river bed erosion and associated sediment transport control the relief of tectonic landscapes and sedimentary fluxes (e.g., Whipple and Tucker, 2002), erosion by turbidity currents, along with debris flows (denser flows in which particles are held in suspension by a viscous matrix), mass movements (landslides), and effects of oceanographic currents (Shepard, 1981), dictate the incised relief of continental slopes and sediment transfer to the continental rise and abyssal plains. In the new sonar data becoming available, continental slope canyons are indeed morphologically similar to subaerial erosional systems in both visual and quantitative senses (McGregor et al., 1982; Mitchell, 2004, 2005; Pratson and Ryan, 1996). Recent attempts have been made to model slope canyon morphology by adapting stream-power erosion laws now popular in fluvial geomorphology to submarine erosion (Mitchell, 2004, 2005). Although such models can explain aspects of canyon morphology, such as the concave-upward long profiles of U.S. Atlantic canyons, they rely on assumptions of how sedimentary flows originate (e.g., from slope failure in canyon walls) that are difficult to verify quantitatively. In contrast, canyons with large through-put compared with their eroded mass, such as the sections of canyons studied here (Fig. 1), suffer less from this complication and present an alternative way to isolate parameters controlling erosion rate. In particular, the geometry of knickpoints can potentially reveal the extent to which the style of erosion is detachment-limited or transport-limited, depending on whether they advect or smooth out, respectively (e.g., Whipple and Tucker, 2002).

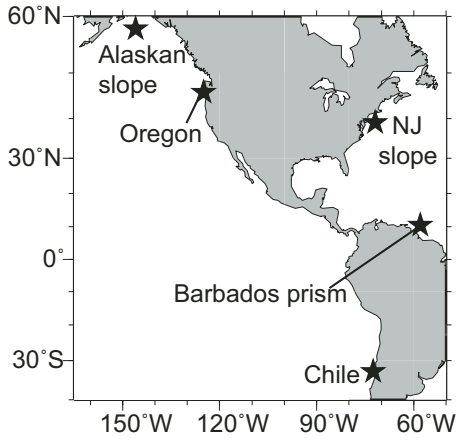

Figure 1. Locations of the studied data sets. NJ—New Jersey.

†E-mail: neil@ocean.cardiff.ac.uk.

GSA Bulletin; May/June 2006; v. 118; no. 5/6; p. 589–605; doi: 10.1130/B25772.1; 12 figures; Data Repository item 2006065.

These studies have implications for the details of stratigraphy and mass transfer within accretionary prisms. Whereas isolated prisms typically have only veneers of slope sediment, those close to continents can have significant thicknesses (e.g., 30% off Costa Rica; Shipley et al., 1990). Whether turbidity currents deposit sediment in piggyback basins on the prism or whether they bypass to the trench depends in part on whether channels maintain continuous downgradient profiles. Localized tectonic uplift can block channels and lead to abandonment (Huyghe et al., 2004). Continuity or abandonment likely depends on many factors, such as flow frequency, vigor, duration, and occurrence relative to tectonic uplift history, whether the transported particles are abrasive, and on the substrate's susceptibility to erosion. The different styles of knickpoint evolution implied by the detachment- and transport-limited models described in the following sections could lead to geometrically different drawdown of topography around the exit channels of piggyback basins, potentially affecting the stratigraphy within basins and hence tectonic signals that can be inferred from stratigraphy. These issues also apply to slope basins created by salt or shale tectonics (Adeogba et al., 2005; Prather, 2003). An indication of the likely mathematical form of the erosion law would be further useful for incorporating erosion into numerical models for how stratigraphy develops at continental margins (e.g., Pirmez et al., 1998; Steckler et al., 1999).

The schemes considered here for modeling morphology are similar to those used in fluvial geomorphology, because smooth abraded surfaces and blocks quarried along joint planes observed in some submarine canyons (McHugh et al., 1993; Robb et al., 1983; Shepard, 1981) suggest that erosion by turbidity currents and debris flows can involve similar abrasion, plucking, and quarrying such as occurs in river beds (Hancock et al., 1998; Whipple et al., 2000). Furthermore, observations in many submarine channels have revealed large-scale erosive scours, flutes, and trenches (Farre and Ryan, 1985; Gee et al., 2001; Hughes Clarke et al., 1990; Klaucke and Cochonat, 1999; Klaucke et al., 2000; Malinverno et al., 1988; Normark and Piper, 1991; Piper et al., 1999; Robb et al., 1983; Ryan, 1982; Shor et al., 1990). Some appear to be the result of bed shear failure under the influence of flow stress (e.g., Klaucke and Cochonat, 1999), a process not unlike that of quarrying in which river flow stress works against friction on joints (Hancock et al., 1998). Shear failure is also implied by sheets of material removed leaving peripheral bedding planes exposed (Piper et al., 1999). Alternatively, scours may be excavated by concentrated abrasion by particles (Shor et al., 1990), in which case scour depth should also be related to flow vigor, amongst other factors. Scours can occur in the lee of obstacles (Hughes Clarke et al., 1990), presumably created by the kinetic energy of suspended particles where detached flowlines reattached to the bed, which is similar to the spatial concentration of abrasion observed in the lee of river boulders (Hancock et al., 1998). Furrows are also common (Piper et al., 1999, 1985), which Farre and Ryan (1985) likened to the effect of snow avalanche furrows and which are thought to be caused by relatively coherent flows (debris flows or slides).

In fluvial geomorphology, reach-scale bed erosion rate is often modeled as a simple function of either bed gradient or curvature, depending on whether the erosion is detachment-limited or transport-limited, respectively. In detachment-limited models, the rate at which particles are removed from the bed is related to the flow shear stress (Howard, 1994) or power (Seidl et al., 1994). Erosion rate is then related to bed gradient, which dictates the vigor of the flow, and can be shown to lead to advection (migration) of knickpoints (Whipple and Tucker, 2002). In transport-limited models (e.g., Tucker and Whipple, 2002), material is easily detached from the bed, and erosion rate is then governed by variations in transport flux of the stream, which lead to diffusive-like bed changes (related to the degree of long-profile curvature, with downward and upward curvature leading to erosion and deposition, respectively).

In this study, similar models are presented for submarine erosion, and their results are compared against the morphologies of canyon floor knickpoints created by faulting or folding. Apart from deposition due to converging bedload, the models do not allow for deposition; they are intended only to represent erosion ("accumulative flow"; Kneller, 1995). To simplify them, flow is assumed to be locally at equilibrium (not accelerating), because this allows flow properties to be related to local bed gradient. The smaller knickpoints studied here are affected by backwater (nonequilibrium) effects that are not well represented by such models, but compiling knickpoints with a range of scales may provide a sense of the transition to equilibrium conditions. A further difficulty is that knickpoints could potentially arise during simple entrenchment because of varied resistance of the substrate to erosion (Miller, 1991). As detailed ground-truth data are generally lacking, such a possibility cannot be ruled out for individual knickpoints, but some occur in channels eroded through trench and piggyback basin fill turbidites, where an explanation in terms of isolated resistant substrates seems unlikely. A time progression in the abandonment of strath or other terraces (Burbank and Anderson, 2001) would be desirable to demonstrate migration less equivocally. Further, as induration and compaction typically increase with burial depth in trench turbidites, aside from local overpressure effects (e.g., Bray and Karig, 1986; Screaton et al., 2002), knickpoint relief is unlikely to be controlled by resistant caps (Holland and Pickup, 1976). Knickpoint interpretation is also complicated, because no data set yet exists to constrain fully the history of tectonic motion and of the through-canyon sediment flux and properties of the flows. Nevertheless, by compiling a large body of data, we can get a sense of the diversity of knickpoint morphology and can discuss possible causes. The survey presented herein provides evidence that the lips of small knickpoints vary from sharp to rounded, a result that implies the varied influence of a number of factors, whereas the largest knickpoints studied (from the Barbados prism) have rounded lips, suggesting at least a component of diffusion.

CHANNEL BED EROSION MODELS

Although submarine channels can appear similar to stream networks, the dynamics of turbidity currents are likely to differ in a number of respects from streams (Peakall et al., 2000), which complicates the study of how flow and substrate properties determine bed erosion rate and also the ability to discriminate between detachment- and transport-limited models from morphologic data. The excess density of the flow with ambient water is much smaller than for river water with air, so relatively minor changes in solid load arising from erosion or deposition can significantly change flow velocity, leading to feedbacks with erosion (Parker et al., 1986). Some numerical models (Fukushima et al., 1985; Pantin, 1979; Parker et al., 1986) represent how changes in velocity arise from pickup of loose, unconsolidated bed material. Their complexity illustrates that flow velocity near source regions will be difficult to reconstruct, for example because sediment entrainment rates are sensitive functions of grain size and other properties that are poorly known for the prehistoric flows responsible for erosion. Turbidity currents can originate from dilution of debris flows (Mohrig and Marr, 2003), hyperpycnal outflow of muddy river water (Mulder and Syvitski, 1995), or storm agitation (Wright et al., 2001), also adding uncertainty to reconstruction of flow properties near the source. Furthermore, flows produced by failure of canyon wall deposits are likely to lead to a progressive increase in frequency and erosive effects downcanyon (Mitchell, 2004). Deriving information on how erosion rate is controlled by substrate

or flow properties from morphology is therefore problematic for proximal regions. In this study, field examples were sought far from flow sources, where relative changes in sediment load over the short sections studied were expected to be minor, so that an assumption of conservative sediment flux could be adopted. Relative changes in frequency of flows arising from canyon wall failures (Mitchell, 2004) should also be minor.

Detachment-Limited Erosion Models

In these models, erosion is constrained by the rate at which material is removed from the bed, while the resulting sediment is efficiently transported away, so that it is unable to form an armoring. Elevation changes in an artificially generated badland suggested (Howard and Kerby, 1983) that erosion rate was proportional to the bed shear stress, τ_b, imposed by the streams. Allowing erosion only above a threshold stress τ_0, erosion rate, E, can be written (e.g., Foster and Meyer, 1975):

$$E \propto (\tau_b - \tau_0)^n; \text{ for } \tau_b > \tau_0, \quad (1)$$

where the exponent n allows for nonlinearity. As $\tau_b \propto u_*^2$ and $U \propto u_*$ (e.g., Webber, 1971) (u_* is the near-bed shear velocity [$u_* \equiv \sqrt{(\tau_b/\rho_w)}$], the erosion rate $E \propto (U^2 - U_0^2)^n$ (where U_0 corresponds to τ_0).

The momentum equation for a steady particle-laden current of uniform width (Fukushima et al., 1985; Parker et al., 1986) is:

$$\frac{\partial U^2 h}{\partial x} = -\frac{1}{2} Rg \frac{\partial Ch^2}{\partial x} + RgChS - u_*^2, \quad (2)$$

where U and C are flow depth–averaged speed and sediment volumetric concentration, respectively, h is the flow thickness (m), g is the acceleration due to gravity (m/s^2), R is the submerged particle specific gravity [$(\rho_s - \rho_w)/\rho_w$ or ratio of sediment particle buoyant density to water density ρ_w], and S is bed gradient (positive with declining elevation downstream). The left-hand term in equation 2 represents the fluid acceleration, including both acceleration of the flow and ambient fluid entrained into the flow (i.e., $U^2\partial h/\partial x$). The three terms on the right represent stresses acting along the direction of flow due to static pressure gradients caused by variations in sediment concentration or flow thickness, flow weight, and bed friction, respectively,

Although progressive flow inflation associated with water entrainment means that turbidity currents never strictly reach equilibrium, a quasi-equilibrium state in which accelerations are minor can be envisaged, greatly simplifying the analysis. For a steady current on a long, uniform slope, the flow velocity U can be calculated from equation 2 by expanding the first derivative and setting $\partial U/\partial x = 0$ and $\partial Ch^2/\partial x = 0$ so that:

$$u_*^2 + U^2 \partial h/\partial x = RgChS, \quad (3)$$

retaining the entrainment part $U^2\partial h/\partial x$ of the total acceleration $\partial U^2 h/\partial x$. As $u_*^2 = C_d U^2$, where C_d is a friction coefficient, and at quasi-equilibrium, the entrainment rate $e_w = \partial h/\partial x$ (Pirmez et al., 2000) equation 3 can be rearranged to a form similar to the familiar Darcy-Weisbach or Chezy formula (e.g., Komar, 1969):

$$U = \left(\frac{RgChS}{(C_d + e_w)} \right)^{1/2}. \quad (4)$$

In equation 4, the entrainment coefficient e_w has a similar role to the bed friction factor C_d, i.e., entrainment stress is equivalent to a friction stress.

To allow for changes in C and h from water entrainment and changes in speed, a uniform sediment flux assumption is applied (Komar, 1977). As sediment flux $Q_s = CRhWU$, where W is the effective flow width (m), substituting CRh in equation 4 and rearranging yields:

$$U = \left(\frac{gQ_s S}{W(C_d + e_w)} \right)^{1/3}. \quad (5)$$

Thus, U becomes a function of mainly S and W, as g and Q_s are constant here, although C_d may vary because of varied bed roughness. Water entrainment rates, and hence e_w, are expected to increase on steeper slopes and with larger densimetric Froude numbers as the upper interface becomes unstable (Middleton, 1966b). According to Parker et al. (1986), e_w can be estimated from the flow Richardson number Ri:

$$e_w = 0.00153/(0.0204 + Ri), \quad \text{where } Ri = RgCh/U^2. \quad (6)$$

Above a critical Ri (¼ according to Wright et al., 2001), entrainment is small and the quasi-equilibrium formulae apply (Parker et al., 1986). Assuming a typical excess density $\Delta\rho$ = 50 kg/m^3, Pirmez and Imran's (2003) reconstructed flow velocities and thicknesses in the upper Amazon fan channel (S = 0.4) all imply Ri > 1, but Ri < ¼ if $\Delta\rho$ < 2–4 kg/m^3. Although $\Delta\rho$ is poorly known in general, estimates of $C = 10^{-3}$ to 10^{-1} and velocities summarized by Normark and Piper (1991) suggest that Ri < ¼ is possible for flows on steep gradients. Thus, entrainment can be considered to modify equation 5 by causing $e_w(S, W, C_d)$, i.e., it mostly modifies the sensitivity of U to local gradient and will be a small effect if $C_d > e_w$, as usually is assumed. If the flow is not at equilibrium, variations in h from entrainment can affect other parts of the flow because of the pressure term in equation 2.

Ignoring temporarily the threshold of erosion, and incorporating g, Q_s, C_d, and e_w into K_a, equations 1 and 5 suggest that:

$$E = K_a (S/W)_{2n/3}. \quad (7)$$

K_a also encompasses factors representing bed erodibility and other rate factors, such as turbidity current frequencies, durations, and the nature of solid load if eroding by abrasion. If E is proportional to shear stress (Howard and Kerby, 1983), n = 1. E is proportional to specific flow power (Seidl et al., 1994), the gradient exponent $2n/3 = 1$.

Some rivers and their associated valleys narrow where crossing regions of more rapid tectonic uplift (Duvall et al., 2004; Lavé and Avouac, 2001) or growing anticlines (Harbor, 1998), and channel narrowing has been observed across knickpoint faces in stream table experiments (Gardner, 1983). According to Finnegan et al. (2005), narrowing occurs because fast flow on steep gradients is accompanied by a decreased flow cross-sectional area if discharge is conserved. Their predicted width variation for rivers is:

$$W = [\alpha(\alpha + 2)^{2/3}]^{3/8} Q^{3/8} S^{-3/16} n_m^{3/8}, \quad (8)$$

where α is the channel width-to-depth ratio and n_m is Manning's roughness coefficient. Although the data presented here have not been analyzed to work out $W(S)$, some of the submarine channels narrow where crossing active anticlines and steep knickpoints. Supposing that the tendency can be represented by a simple correlation ($W \propto S^{-p}$, where p is a constant exponent), equation 7 simplifies to:

$$E = K_a S^{2n/3(1+p)}. \quad (9)$$

In rivers, other factors affect erosion rate, such as abundance of tools in the flow and bed armoring when bedload is excessive (Sklar and Dietrich, 2001). If bedload is removed efficiently on steep gradients, the tools effect could vary spatially, but, as there are no independent data to constrain bedload cover, this effect can only be considered qualitatively in the interpretation. This approach also ignores the possibility that channels crossing active anticlines respond to steepening by changing their plan-view geometry, such as sinuosity or braiding (Ouchi, 1985). Further, because of the patchy nature of canyon floor scours, erosion is irregular, and equations such as equation 9 based on reach-scale gradient

are simplified, as is also the case for river bed erosion models (Hancock et al., 1998). The assumption is effectively made that scouring occurs in different places throughout the history of channel development so that the equations represent erosion in a long-term average sense.

Transport-Limited Erosion Models

In these models, bed material is efficiently detached and erosion rate is controlled by the rate at which bedload transport flux is varied by the flow (e.g., Tucker and Whipple, 2002). The diffusive-like evolution of bed topography predicted by such models has been observed in experimental and natural alluvial streams (Begin, 1988; Begin et al., 1981; Cui et al., 2003; Lisle et al., 1997; Paola, 2000). Dunes and ripples commonly found in submarine channels (Hughes Clarke et al., 1990; Klaucke et al., 2000; Malinverno et al., 1988; Normark and Piper, 1991; Piper et al., 1988; Shor et al., 1990) suggest that some transport occurs as bedload, so variations in bedload flux could also significantly affect submarine channel bed topography.

According to Soulsby (1997), the bedload transport formula originally developed by Bagnold (1963) is still considered reasonably accurate for marine sands:

$$Q_b \text{ (kg/m/s)} \propto \tau_b^{1/2}(\tau_b - \tau_0); \text{ if } \tau_b > \tau_0. \quad (10)$$

Simplifying the equation by ignoring the threshold and substituting u_*^2 for τ_b, gives transport flux Q_b (kg/m/s) $\propto u^{*3}$. The continuity relation (conservation of mass) relates erosion rate to lateral changes in transport flux:

$$E = 1/\rho_s \, \partial Q_b/\partial x, \quad (11)$$

where ρ_s is the dry bulk density of bed sediments (kg/m^3). Substituting $u_* \propto U \propto (S/W)^{1/3}$, derived earlier, into $Q_b \propto U^3$ suggests simply $Q_b \propto S$ (letting W and ρ_s be constant for simplification). Since gradient $S \equiv -\partial z/\partial x$, differentiating in x and substituting for $\partial Q_b/\partial x$ in equation 11 leads to a diffusion equation in z (bed elevation):

$$E = -\partial z/\partial t = -K_d \, \partial^2 z/\partial x^2. \quad (12)$$

K_d incorporates various constants of the above relations (including a constant of proportionality of equation 10) and effects of flow frequency and duration as before with K_a.

Additional effects mean that the true bed evolution could be more nonlinear than implied by equation 12. For example, recirculating flume experiments on sands have documented gravitational effects on bedload (Damgaard et al., 2003). In those experiments, sand flux was monitored while water flow rate was controlled and longitudinal gradient varied. Bedload flux changed by 2–3× when gradient was varied from −20° to +20° at a flow speed of 0.35 m/s measured at 13 cm above the bed but was invariant with bed gradient at speeds of 0.65 m/s. As equation 12 represents only continual bedload transport, it does not account for transformation of bedload to suspended load by breakdown of particles or with increasing flow stress (e.g., Bagnold, 1963; Dade and Friend, 1998). This cannot be predicted without more detailed knowledge of the eroded sediment texture and flow stresses.

Morphologic Predictions of the Models

Many of the following comments repeat those made previously (Howard, 1994; Rosenbloom and Anderson, 1994; Seidl et al., 1994; Stock and Montgomery, 1999; Tucker and Whipple, 2002; Weissel and Seidl, 1998). The simulations in Figure 2 illustrate the topographic evolution expected from the models. They were created using finite difference calculations with an inverted error function as the initial condition representing the outer slope of an anticline or a fault (escarpments typically degrade rapidly to leave a rounded base and lip rather than a sharp profile; Mitchell et al., 2000). Parameter values are omitted here for brevity, and the scales are arbitrary; the intent is merely to show the style of morphological change rather than any particular knickpoint. Equation 9 with the slope exponent $2n(1 + p)/3 = 1$ has a simple traveling wave solution so that knickpoints generated instantaneously should have the same form as their initial topography but are translated upstream (Fig. 2A). If $2n(1 + p)/3 < 1$, propagation speed is greatest where gradients are small. This rounds off the lip and reduces knickpoint relief with time (Fig. 2B). If $2n(1 + p)/3 > 1$, the lip becomes sharp, because propagation speed is greatest where gradients are steep, which undermines the lip (Weissel and Seidl, 1998). Diffusion reduces knickpoint relief and gradients, and also broadens the knickpoint's spatial extent (Fig. 2D), but involves no translation.

A threshold of erosion or transport can significantly affect channel-long profiles (Snyder et al., 2003; Tucker, 2004; Tucker and Bras, 2000). This is illustrated in Figures 2C and 2E by imposing a gradient threshold for erosion rate and transport flux, respectively. In deriving Figure 2C, the simplification has been made that equation 1 can be equally written, given the uncertainties in the erosion process, by $E \propto \tau_b^n - \tau_0^n$ (Tucker, 2004). Similarly, equation 10 can be simplified by writing $Q_b \propto \tau_b^{3/2} - \tau_0^{3/2}$, which implies $Q_b \propto (S - S_0)$ for a constant-width channel ($p = 0$). Erosion and deposition in Figure 2E were then calculated by applying the continuity relation (equation 11). As can be seen from the graphs, either a detachment- or a transport-limited scheme with a threshold produces a more angular lip. Considering that the flows in reality impose various stresses relative to the threshold, the effect will be less defined, but the lip should still become more angular than in the absence of a threshold.

These predictions are clearly idealized, but their differences with real turbidity currents can be anticipated to some extent and allowed for in interpretation. For example, varying C_d or e_w alters the erosion or transport flux responses to gradient (hence differences such as those seen in Figs. 2A and 2B probably cannot be discriminated). Sediment is deposited within piggyback basins where flows have low velocity and over-spill their channels. The upper reaches in Figure 2 should therefore be aggradational, whereas seismic reflection data from knickpoint faces studied here show that they are erosional. Depending on the rate of aggradation compared with erosion, these effects could round knickpoint lips.

Nonequilibrium Flow

For short distances over which stream-wise accelerations are important, equations 9 and 12 no longer represent erosion, because bed shear stress is decoupled from local bed gradient. Simulations of field turbidity currents (Skene et al., 1997; Pratson et al., 2000) show them approaching equilibrium over distances of one or more kilometers, and in experiments (Garcia and Parker, 1989; Garcia, 1993), equilibrium is approached over distances that are an order of magnitude larger than flow thickness. G. Parker (2005, personal commun.) suggests that the ratio h/S provides a rough estimate of this backwater length scale for streams. For a typical flow of h = 100 m and steep gradient S = 0.1, the backwater length scale is 1 km. For estimated S and h, flow in many of the small knickpoints studied here are not in equilibrium, and knickpoint morphologies should not be compared simply with those of the simulations in Figure 2. Some effects of accelerations are as follows.

Equation 2 suggests what happens where a turbidity current crosses to a steeper gradient (i.e., across a knickpoint lip). The flow accelerates because of the increased weight term $RgChS$. If entrainment is gradual, the faster flow on a steep reach will be thinner to conserve discharge, which causes a pressure gradient along the direction of flow ($\partial h/\partial x$ negative), reinforcing acceleration in the drawdown (upper) reach. If water entrainment is considered, inflation of

the current will tend to oppose acceleration by reducing the pressure term in equation 2, but otherwise these are comparable effects to those that occur across steepening gradients of streams (Webber, 1971).

In stream table experiments (Gardner, 1983), acceleration in the drawdown reach caused erosion above the lip, a feature observed in some rivers (Bishop and Goldrick, 1992). With erosion also at the top of the knickpoint face, this led to knickpoints progressively losing their relief and flattening ("slope replacement"; Gardner, 1983). If the knickpoint face is nearly vertical (a headcut), the flow can separate from the bed, and kinetic energy excavates a plunge pool, leading to a more complex evolution (Stein and Julien, 1993).

Over-spill or flow stripping of the current as it expands with entrainment might be expected to be important also. However, in the areas considered, the flow passes from a shallow piggyback basin channel to a deeper canyon, so it becomes more confined. Furthermore, turbidity currents are expected to be strongly density stratified (Altinakar et al., 1996; Chikita, 1990; Garcia, 1993; Normark, 1989; Stacey and Bowen, 1988). Peakall et al. (2000) used Altinakar et al.'s data to show that removing 50% of the top of such a flow should reduce its velocity by only 5% because of its small contribution to the flow's average density and weight.

Below the knickpoint, a hydraulic jump is possible if the flow slows from supercritical to subcritical (Komar, 1971). Laboratory experiments (Garcia and Parker, 1989) have illustrated how an abrupt slowing beyond the jump can lead to deposition of bedload, whereas suspended loads can be carried farther depending on their settling velocity. Material eroded from the knickpoint face could potentially accumulate in the lower reach if not disaggregated and carried away in suspension. Experiments on even subcritical flows have shown decreased deposition just beyond a break of slope caused by enhanced turbulence (Gray et al., 2006). Thus, the knickpoint lip rather than base is interpreted here from observations.

SONAR DATA SETS

This study draws on multibeam echo-sounder data of canyons principally on active margins (Fig. 1). Most of the data were collected on U.S. ships and provided by the National Geophysical Data Center (NGDC, Boulder, Colorado). Data in Figures 3, 4, 5, and 6 were collected with 1980s-generation SeaBeam systems, whereas data in Figure 7 and Figure 6 north of 46°01′N were collected with a more recent generation of that instrument. The data from the Barbados channels were taken from published Figures (Huyghe et al., 2004) derived from Simrad EM12 multibeam data collected on a French vessel. Aside from Figure 3 (from the NGDC Coastal Relief Model, which was provided as a grid), the data were binned to reduce noise and interpolated onto grids using surface fitting software (Smith and Wessel, 1990) before being displayed in shaded relief and with depth contours for interpretation. Because of differing noise characteristics, different grid resolutions were chosen: (east-west × north-south) 77 × 111 m (Astoria), 279 × 222 m (San Antonio), 114 × 111 m (Alaska), and 72 × 92 m (New Jersey). Channel paths were manually digitized and sampled by linearly interpolating between grid nodes along those paths.

Because of difficulty and cost, very limited areas of sonar data such as these have corresponding ground-truth data. Interpretation is instead guided by knowledge of how artifacts arise, such as from motion-sensor problems, erroneous sound velocity measurements, sounding noise, leakage of strong reflected signals into off-specular beams, or delayed response of bottom detection range gates to depth changes (de Moustier and Kleinrock, 1986; Hughes Clarke et al., 1996). These artifacts are usually not dominant, however; comparisons with higher-resolution bathymetry have shown that multibeam data collected without obvious blunders are essentially low-pass versions of the true seabed topography but with a small uncorrelated noise component superimposed (Goff and Kleinrock, 1991). Noise represented by obvious outliers can easily be interpreted (e.g., Fig. 7). Similarly, the NGDC Coastal Relief Model (Fig. 3) incorporates older soundings that form isolated anomalies, which can be easily interpreted.

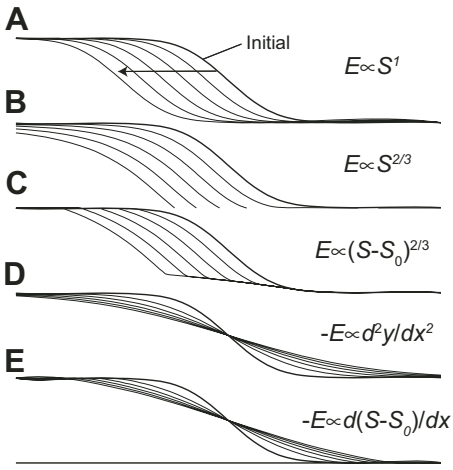

Figure 2. Predicted styles of knickpoint evolution if erosion and deposition were to follow various simple rules. The one-dimensional (1-D) simulations were developed using finite difference calculations with an inverted error function as the initial condition (bold lines). (A) If erosion rate is linearly proportional to gradient (proportional to flow power), the channel topography simply migrates. (B) If erosion rate is proportional to $S^{2/3}$ (proportional to bed shear stress), the knickpoint face migrates but with the lip progressively rounding. (C) If erosion only occurs where the gradient exceeds a threshold S_0, the knickpoint face retreats, but the lip sharpens. (D) If erosion and deposition are governed by the flow's ability to transport bedload, the knickpoint progressively diffuses without retreating. (E) If bedload transport only occurs above a gradient threshold S_0, the knickpoint adopts a sharp lip and a face at close to the threshold gradient.

OBSERVATIONS OF KNICKPOINTS AND CANYON RELIEF

The following first describes the small-scale knickpoints (extents are smaller than backwater length scales) and then the larger Barbados channels, which form the basis for erosion modeling.

New Jersey Continental Slope

Circular embayments within the middle and lower slope of the New Jersey continental slope resemble landslide headwalls (Farre et al., 1983; McAdoo et al., 2000) that formed abrupt knickpoints (Fig. 3). Their origin has been controversial. Robb (1984) argued that they resulted from spring sapping and chemical erosion of carbonates, whereas McHugh et al. (1993) suggested that opal-A to opal-CT transformation of silica within the chalk caused exfoliation. McHugh et al.'s observations of hard siliceous porcellanite chalk and more friable chalk outcrops during two submersible dives are reproduced against profiles 1 and 2 in Figure 3. They suggested that the less silica-rich chalk eroded more easily, leaving porcellanite chalk forming knickpoint lips. This is shown imperfectly in the two profiles in Figure 3, but dive observations were projected onto the profile assuming a possibly inaccurate nearly horizontal stratigraphy (Robb et al., 1981). The interpretation of the embayments as landslide headwalls is considered the most convincing here, based on associations with slide deposits (McAdoo et al., 2000) and that their broad lower canyon floors lie parallel to strata, as would be expected from structurally controlled slope failure (Farre, 1987), although the outcrops have

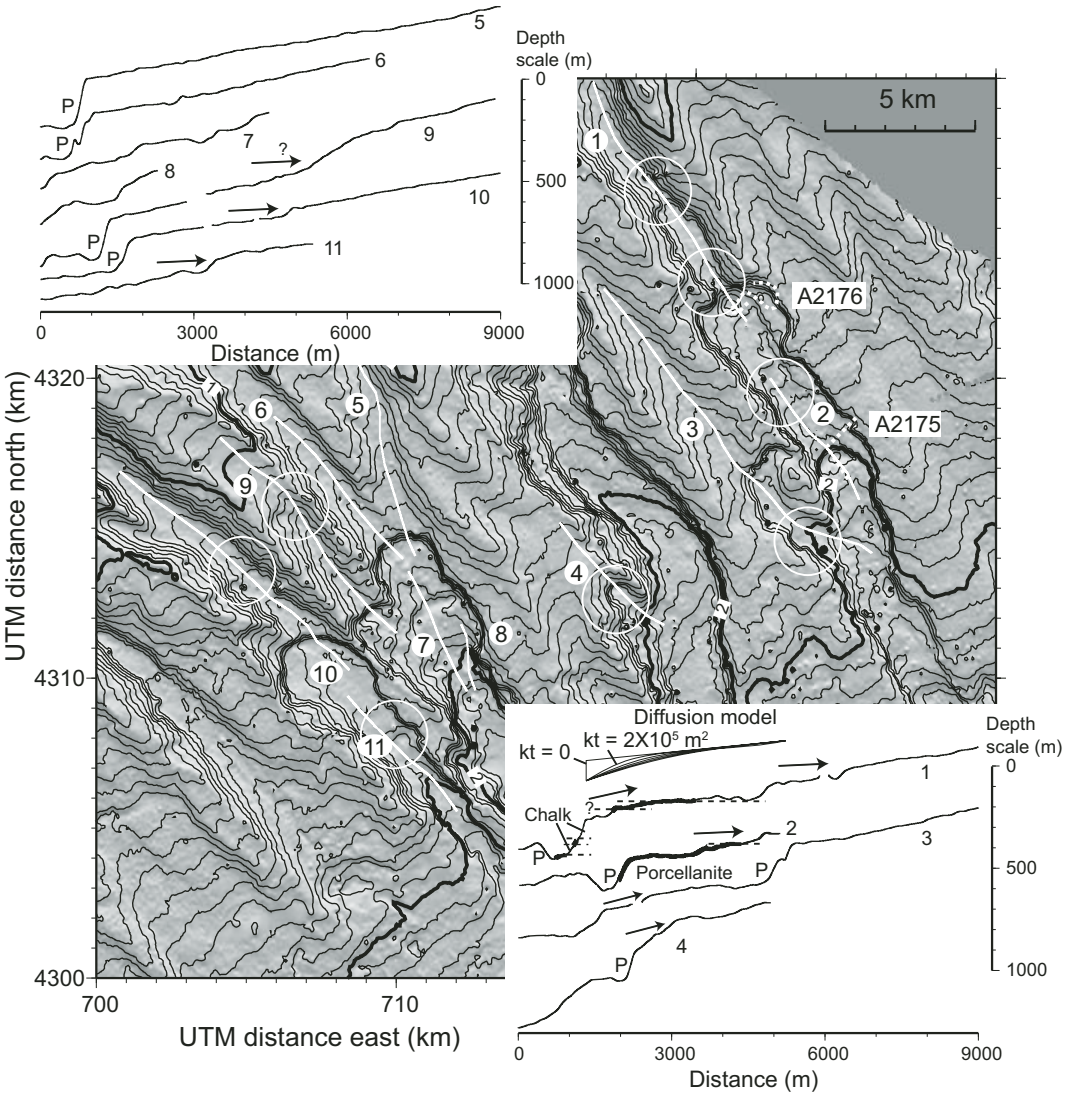

Figure 3. Bathymetry of the U.S. Atlantic continental slope off New Jersey collected in 1989 with a SeaBeam multibeam sonar on R/V *Atlantis II* (W.B.F. Ryan, chief scientist) and made available by the National Geophysical Data Center (Coastal Relief Model). The data are plotted in a Universal Transverse Mercator Projection (zone 18). Depth contours are every 50 m, with every 1000 m annotated in kilometers (bold contours with numbers on rectangular white tiles). The two dotted lines marked A2175 and A2176 are submersible dive tracks. Large open white circles mark knickpoints. Also shown by the white lines is a series of channel profiles annotated 1 to 11 (on elliptical white tiles). Their profiles are plotted with a 4:1 vertical exaggeration in the two insets, which also include possible associated knickpoints (arrows) and plunge pools (P). The porcellanite intervals inferred from submersible operations (McHugh et al., 1993) are marked in bold; dashed lines mark the depths of the porcellanite-chalk transitions observed (the upper transition for profile 1 was projected from A2176, assuming that the stratigraphy was nearly horizontal; Robb et al., 1981). Also shown above the profiles in the lower-right inset is a series of solutions to equation 13, illustrating that knickpoint topography has clearly not evolved according to a simple diffusion equation.

Figure 4. (A) Bathymetry of the lower Gulf of Alaska continental slope collected with a SeaBeam multibeam sonar of National Ocean Service ship *Surveyor* and made available by the National Geophysical Data Center. Depth contours are plotted every 50 m. General annotations are as in Figure 3. Dotted and medium dashed lines mark the two reference profiles shown with the channel profiles in D. The two bold dashed lines are survey lines of R/V *Lee*, along which U.S. Geological Survey scientists collected seismic reflection data in 1981 (lines 13 and 14 of Fruehn et al. [1999], chief scientist R. von Huene). (B–C) Interpretations of seismic reflectors adapted from Fruehn et al. (1999) for lines *Lee*-13 and *Lee*-14, respectively. Locations are shown in A. Only the near-surface reflectors and interpreted thrust faults are shown to compare with the bathymetry. Nomenclature (A1, etc.) follows the annotation of anticlines by Fruehn et al. The line 14 anticlines are reproduced on A. A, B, and C have equal horizontal (distance) scales. (D) Channel profiles along the continuous white lines marked in A. Although aligned at the frontal thrust, distances are shown along each profile (not projected along a common line), so individual features do not line up exactly.

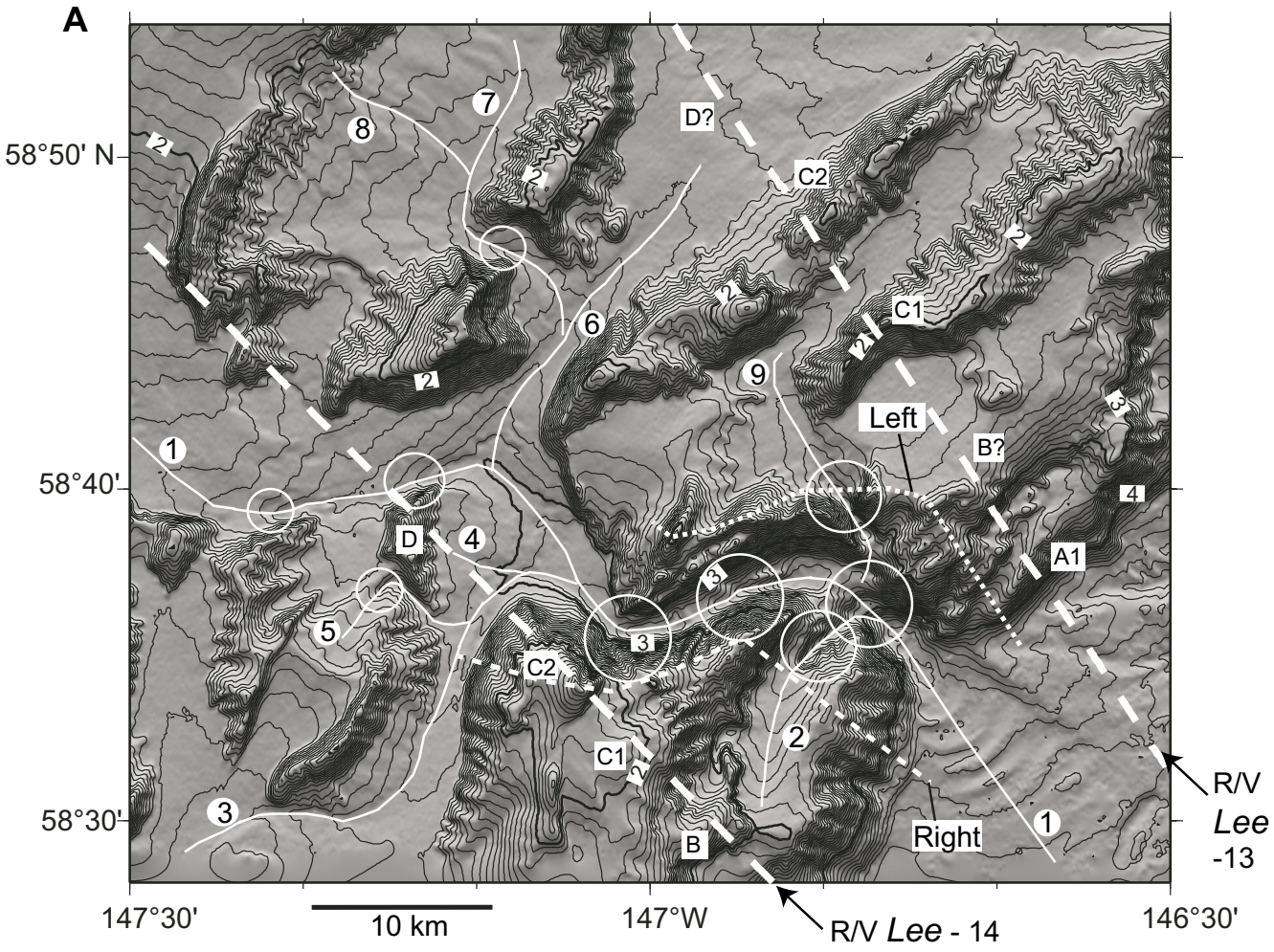
A
58°50' N
58°40'
58°30'
147°30'
10 km
147°W
146°30'
R/V Lee - 14
R/V Lee -13
D?
C2
C1
B?
Left
Right
A1
B
D
1
2
3
4
5
6
7
8
9

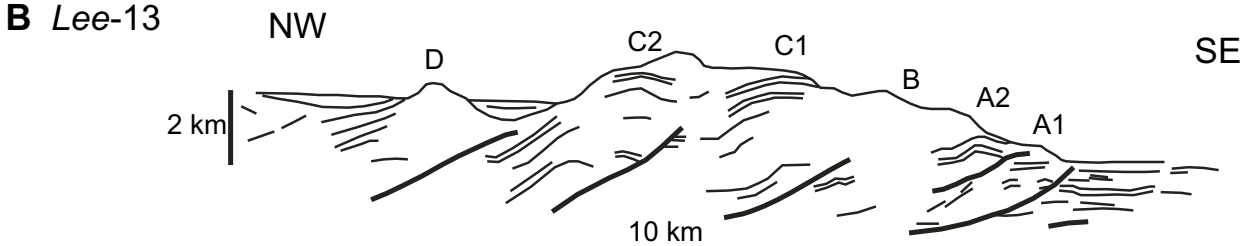
B Lee-13
NW
SE
2 km
D
C2
C1
B
A2
A1
10 km

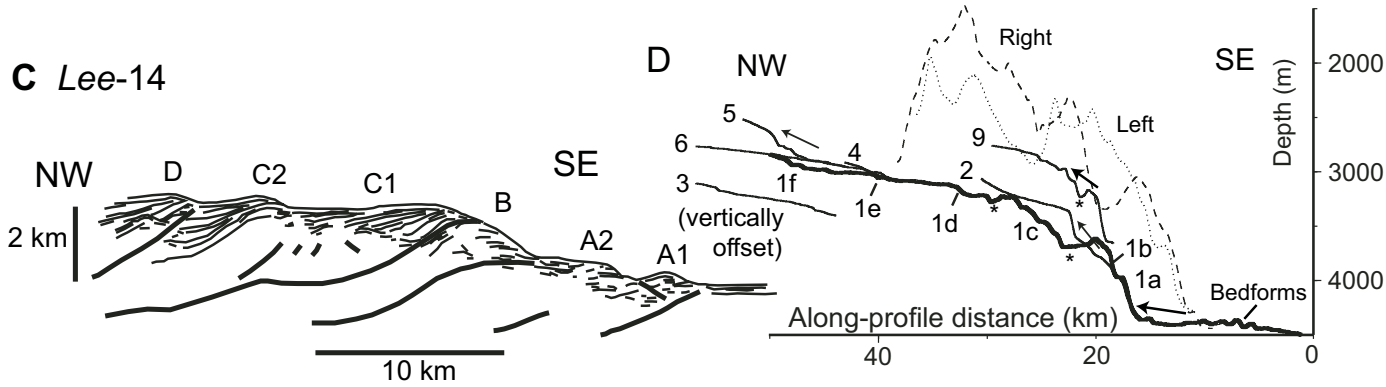
C Lee-14
NW
SE
2 km
D
C2
C1
B
A2
A1
10 km
D
NW
SE
Right
Left
Depth (m)
2000
3000
4000
5
6
3
(vertically offset)
4
1f
1e
9
2
1d
1c
1b
1a
Bedforms
Along-profile distance (km)
40
20
0

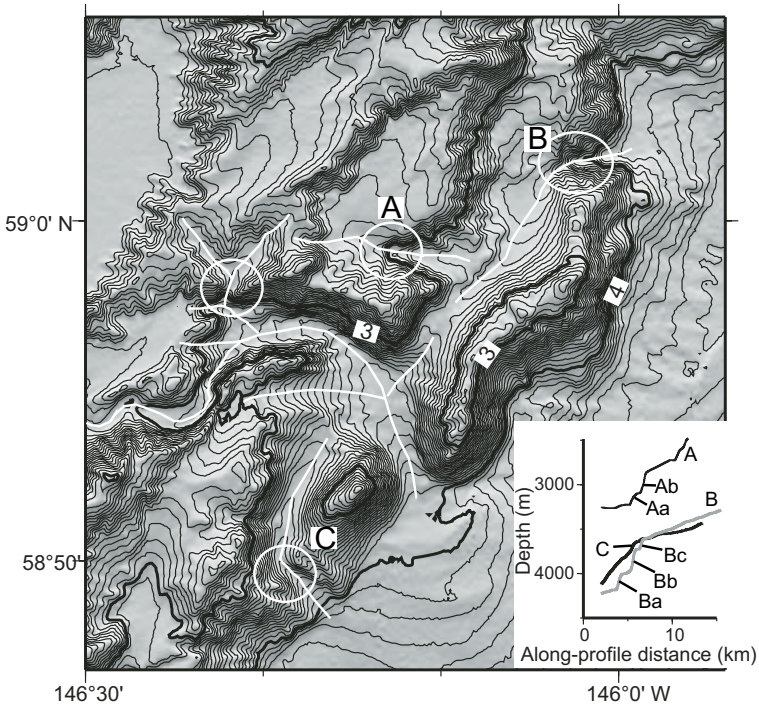

Figure 5. Bathymetry of the Alaskan slope; annotations are as in Figure 4. Lower-right inset shows cross sections along the channels A, B, and C on the map. Knickpoints Aa, Ab, Ba, Bb, and Bc are discussed in the text.

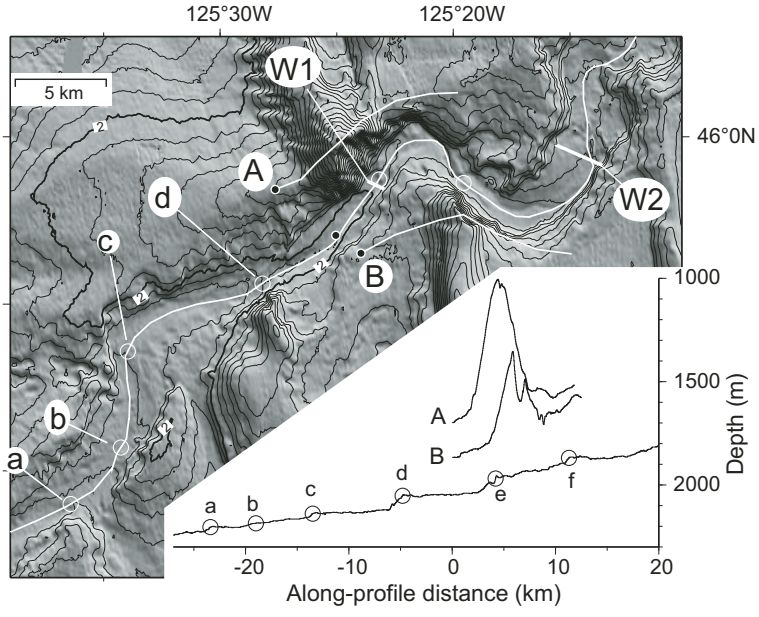

Figure 6. Bathymetry of Astoria Canyon, offshore Oregon. Depth contours are plotted every 50 m, and bold contours are annotated in kilometers. Data were collected (south of 46°01′N) by the National Ocean Service and (north of 46°01′N) on R/V *Melville* (Chris Goldfinger, chief scientist). Inset shows profiles along the two lines A and B, and along the channel marked on the map (distances are relative to the filled circles shown on the map). Open circles on the profile and map locate knickpoints a–f. Bars marked W1 and W2 mark the narrow width of the channel passing through an anticline compared with a piggyback basin.

probably been modified further by exfoliation and dissolution (McHugh et al., 1993).

Figure 3 reveals a number of escarpments separated upstream from the slide headwalls by narrow slots running upslope for distances of 1–2 km (large open circles). Arrows on the topographic profiles (insets to Fig. 3 and in subsequent figures) associate slide headwalls with those escarpments (arrow head). Below the headwalls are depressions (marked "P" on the profiles) interpreted as plunge pools excavated by sedimentary flows (Farre and Ryan, 1985; Lee et al., 2002; McHugh et al., 1993). Since typically $S \approx 0.03$, these are small-scale knickpoints (extents < h/S = 3 km, if h = 100 m).

The fact that the slots are narrower than their host valleys suggests that, whereas the flat or U-shaped floors of the host valleys may originate from slope failure, the slots themselves were eroded by channelized sedimentary flows and that the upslope escarpments are either propagated knickpoints or originate from localized resistance to erosion. Modeling their development would be complicated because of varied resistance to erosion of the different lithologies (McHugh et al., 1993), but a simple diffusive-like evolution of the long-profile knickpoint morphology can at least be ruled out. The model profiles in Figure 3 (lower-right inset) illustrate this for the simplest geometry in which the slope was initially a linear ramp, and the resistant porcellanite outcrop was maintained as a fixed boundary condition. The appropriate solution to equation 12 is (Hanks et al., 1984; Mitchell, 1996):

$$z(x,t) = a\,\mathrm{erf}(x/2\sqrt{(\mathrm{k}t)}) + bx, \qquad (13)$$

where a is the initial erodible layer thickness and b is its original long-profile gradient. The solutions in Figure 3 were calculated using a = 100 m and b = 0.025 (curves are in intervals of $\mathrm{k}t = 2 \times 10^5$ m^2).

Alaskan Slope Area A

Lying within the Gulf of Alaska, the slope is a tectonically active accretionary prism formed at the easternmost Aleutian trench by northwestward subduction of the Pacific plate (Bruns, 1985; Plafker, 1987; von Huene, 1989). The lower slope is composed of off-scraped trench turbidites and hemipelagic sediments and slope sediments, bounded by the Aleutian megathrust. Four dredges from the lower slope immediately northeast of Figures 4 and 5 recovered Paleogene sedimentary rock samples containing reworked material (Plafker, 1987). Glaciation has played an important role in sediment delivery to the margin. According to von Huene (1989), sedimentation rates at Deep Sea Drilling

Project (DSDP) Site 180 (von Huene and Kulm, 1973) in the Alaskan Trench west of the area of Figure 4A have varied by an order of magnitude between glacial and interglacial periods, so sediment flux through the canyons has likely been strongly episodic.

Figure 4A shows bathymetry data of part of the Alaskan slope collected by the National Ocean Service. Figures 4B and 4C show line drawings of seismic reflection data collected along tracks R/V *Lee*-13 and -14 located on Figure 4A. Near-surface reflectors and thrust faults have been adapted from interpretations of Fruehn et al. (1999), who reprocessed the original U.S. Geological Survey data with prestack depth migration.

The bathymetry suggests a complex evolution of sedimentary fill. Some basins have sharp ridges lying perpendicular to tectonic structure (e.g., at the southern ends of profiles 2 and 5 in Fig. 4A), which are possibly a result of sheet-like failure of the sediment (McAdoo et al., 1997). Seismic data do not provide unequivocal evidence for the timing of fault movements, because the stratigraphy depends on the history of sediment supplied to the slope and on how much sediment deposited or bypassed to the trench. The presence of dipping stratigraphy generally and some fanning stratigraphy characteristic of growth faults (e.g., between B and D in line 14), however, suggests that uplift along thrust faults has been generally persistent. On the other hand, sediment within the basins on either side of D on line 13 appears undisturbed, suggesting less activity on this more landward area.

The map and profiles in Figures 4A and 4D reveal many knickpoints with either sharp (e.g., 2) or rounded (e.g., 5) lips. Although the possibility that some knickpoints directly overlie emergent faults cannot be ruled out unequivocally with these data, much of the topography of anticlinal ridges appears to be generated by thrusts along the trench side of each block and by folding. Some knickpoints lie within anticlines (e.g., that beneath the second circle along profile 1, counting upstream from the trench), so they could originate from recent anticlinal uplift or represent compacted or indurated resistant strata brought to the surface. However, many lie upstream of anticline centers, suggesting that they were generated at the anticline and have since migrated upstream, in particular those lying within uniform turbidite fills of piggyback basins, such as along profiles 2 and 5. Although it is difficult to unequivocally rule out varied resistance to erosion as an origin, such examples are more easily explained by migration.

In all cases, knickpoint vertical relief is much smaller than the 500–1000 m relief of anticlinal ridges. The largest relief change is associated

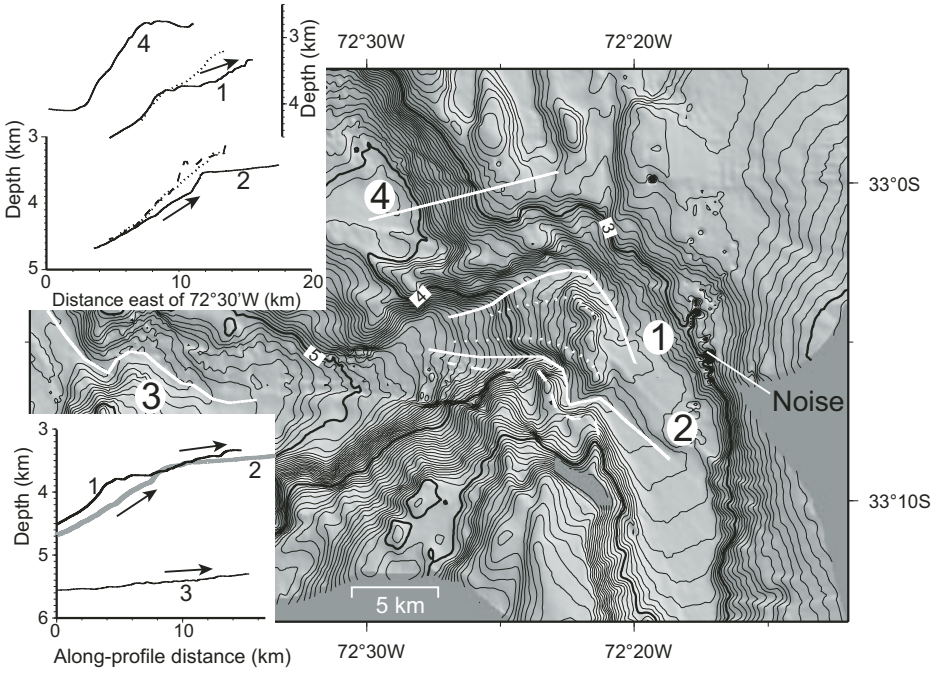

Figure 7. Bathymetry of San Antonio Canyon off Valparaiso, Chile (Hagen et al., 1996). Depth contours are shown every 50 m, with every 1000 m in bold (annotated in km). The lower-left inset shows along-channel profiles, whereas the upper-left inset shows profiles projected to compare channel depths with the adjacent topography (dotted and dashed lines correspond to similar lines on the map).

with two knickpoints located by the trenchward circle of profile 1 (300–350 m and 150–200 m), which lies upstream of the thrust front. Most other knickpoints are 50–150 m. Varied and small relief is potentially a complicated result of episodic tectonic uplift, unsteady erosion associated with episodic sediment flux, or is simply a fortuitous result of multiple emergent faults. Evidence for unsteady sediment flux during ongoing tectonic movements is provided by closed-contour depressions along channels (* in the Fig. 4D). Knickpoints in tributary canyons eroding piggyback basins (e.g., in channels 2 and 9) are interpreted as having been initiated by entrenchment of the main canyon, which led to tributary canyons forming hanging valleys. These knickpoints are also small scale ($<h/S = 70$ km, if $h = 100$ m and with $S = 0.015$). Depressions upstream of the knickpoint face and rounded long profiles, such as for 9, imply entrenchment in the drawdown reach and initial stages of slope replacement (Gardner, 1983).

Alaskan Slope Area B

Figure 5 shows another part of the Alaska multibeam data set, lying to the northeast of Figure 4A. U.S. Geological Survey seismic reflection lines Hinchinbrook and Tact, also processed by Fruehn et al. (1999), lie to either side of this map. They show multiple unconformities and dipping and fanning reflectors, suggesting similar tectonic activity as for *Lee*-13 and *Lee*-14 data. Whereas some knickpoints occur within anticlines, those marked A and B are upstream of anticline centers. Knickpoint Ab has 150 m relief, and adjacent Aa has 50 m relief. Bb has 200 m relief, with knickpoints of 50 and 100 m relief lying upstream and downstream of it. Some knickpoint lips are markedly angular (e.g., Ab in Fig. 5). The drawdown reaches above these lips also appear incised (e.g., A, B, C), as would be expected for small-scale knickpoints.

Astoria Canyon, Oregon State

Astoria Canyon (Fig. 6) (Nelson, 1976) existed before the trenchward anticlinal ridges were formed, and thus it eroded through the ridges as they were uplifted. This is based on seismic reflection data through DSDP Site 174, which show the accretionary wedge nearby overriding earlier fan deposits (Carlson and Nelson, 1987) and the age of fan deposits, which originated at least before 0.76 Ma based on ages at the base of fan deposits recovered at DSDP

Site 174A, or before 1.3–1.4 Ma from the thickness of trench fill (McNeill et al., 2000).

Figure 6 shows the channel passing through anticlines and (west of a line through A-B) the proximal Astoria Fan. East of A-B, the canyon floor narrows where it passes through anticlines at W1 compared with piggyback basins (W2), similar to narrowing of rivers across anticlines. West of A-B, avulsions have created channel-like depressions emanating from the main channel, some of which may be caused by tectonic blocking (e.g., at knickpoint a), and channel sinuosity in general reflects diversion around growing anticlines as is also seen in rivers (Burbank and Anderson, 2001).

Knickpoints a, c, d, and e can be associated with faults or anticlines. Knickpoint a lies at the north end of an anticline, c crosses the channel obliquely but parallel to the anticlines and is probably an active fault line scarp, d lies ~1 km upstream of a small fault escarpment south of the channel, and e may be associated with the escarpment running north-south immediately north of the canyon. Knickpoint b is less distinct and f could have been created by slumping from the north canyon wall. Although the data quality does not allow detailed interpretation, the knickpoints do not show obvious evidence for simple diffusion. The best candidate for migration (d) has a rotated face and sharp lip. Because of the low channel gradient, all knickpoints here are small ($<<h/S$), and the rotated face of d resembles slope replacement.

San Antonio Canyon, Chile

San Antonio Canyon (Fig. 7) lies off Valparaiso in the Chile forearc. Its head, lying close to the mouth of the Rio Maipo, may supply hyperpycnal flows to the canyon (Hagen et al., 1996). In multibeam acoustic backscatter data, ribbons of strong backscatter along the upper canyon floor suggest a braided structure with point bars (Hagen et al., 1996), and therefore flows may not usually occupy the entire floor. The canyon has a large knickpoint of 500–1000 m relief, but its 5-km-wide face is analogous to broad landslide chutes (McAdoo et al., 2000), so it may have originated from landsliding rather than flow erosion.

Two small channels of >100 m relief have been eroded to the north and south of the small north-south topographic ridge lying at the lip of the large-scale knickpoint. The north channel (1) is presently inactive except for exceptional flows, based on the relief of the southern channel forming a barrier to sediment flows from up-canyon. Its long profile (insets to Fig. 7) shows a small 50 m knickpoint upstream of the main escarpment. The southern channel (2) has a knickpoint with a sharp lip where the steep canyon floor has been incised. In the upper-left inset, it could be interpreted to be associated with the relief on the reference profile south of it (dashed line), with a rough translation of that profile landward implying slope retreat. However, the profile below the lip is not a simple translation of adjacent topography. From channel gradients S = 0.025–0.05, these are also small-scale knickpoints, and incision or reduced deposition in the drawdown reach can be interpreted for both channels 1 and 2.

The Southern Barbados Accretionary Prism

Multibeam and seismic reflection data (Faugeres et al., 1993; Huyghe et al., 2004) from the Barbados accretionary prism show canyons eroded through ridges formed by thrust folds (Fig. 8). Turbidity currents that created these canyons originated from Orinoco River sediments and likely contained sands and gravels within the channels and overbank flows of fine sand and silt (Belderson et al., 1984; Faugeres et al., 1993). The seismic data reveal syntectonic fans in hanging walls of the first 2 to 5 frontmost thrust faults, which have been interpreted (Huyghe et al., 2004) as evidence that they were active within the last 500 k.y. Seismic images obtained where the channels traverse thrust folds revealed truncated stratigraphy (Faugeres et al., 1993; Huyghe et al., 2004). Sediment in two cores taken within the canyons was found to be overcompacted, which was attributed to turbidity current flow stresses (Faugeres et al., 1993). Deep-tow sidescan sonar images obtained over the frontmost thrust fold revealed fracture networks (Griboulard et al., 1998). Varied fracture geometry and density and associated diagenetic products (calcretes) (Griboulard et al., 1998) likely created some variability in resistance to erosion. Abundant mud diapirs also occur across the prism, but only one such diapir was mapped (Huyghe et al., 2004), adjacent to the channels studied here (beneath the fold apex c in Fig. 8).

The profiles in Figure 8 (inset) show that, whereas the steep channel reaches tend to be upstream of the steepest parts of the wall profiles, they are also smoother at small scale (2 km) and have less curvature at larger scale (10 km). Erosion therefore appears to have caused both advection and diffusion. For the channel gradients of 0.01–0.02, h/S = 2.5–10 km, so channel c is large scale ($>h/S$) and a and b are marginal. The ratio h/S could be smaller, because some channel depths traversing piggyback basins are only 50 m deep (Faugeres et al., 1993).

Other Channel Knickpoints in the Literature

Knickpoints are present in data from other convergent margins (Kukowski et al., 2001; Orpin, 2004; Soh and Tokuyama, 2002), from intraslope basins affected by salt or shale tectonics (Adeogba et al., 2005; Pirmez et al., 2000; Prather, 2003), where entrenchment of a main canyon has left tributaries as hanging valleys (Mulder et al., 2004; Popescu et al., 2004) and where levees have been breached (O'Connell et al., 1991; Pirmez et al., 2000). In many of these cases, knickpoints lie upstream of a fault or other steep topography (e.g., Tenryu Canyon upstream of Kodai fault; Soh and Tokuyama, 2002), which rules out simple diffusion. Ignoring amphitheater-shaped embayments that may have originated from landsliding (McAdoo et al., 2000), knickpoints in uniform turbidites have various-shaped lips in profile, from rounded to sharp, and lie upstream of steep topography (Adeogba et al., 2005; Kukowski et al., 2001; Pirmez et al., 2000; Prather, 2003). Some authors describe rejuvenation (entrenchment) upstream of newly formed knickpoints (Pirmez et al., 2000; Prather, 2003), suggesting erosion associated with drawdown.

Summary of Observations

Figure 9 shows a selection of knickpoint profiles. The Barbados knickpoints, the largest studied here, are rounded. The other knickpoints are generally shorter and have a variety of lip morphologies, varying from rounded (San Antonio 2, Alaska A/S) to sharp (Alaska A/5, Astoria d). Although hydrodynamic effects prevent these morphologies from being compared directly with the simulations in Figure 2, many knickpoints lie upstream of steep topography within uniform turbidites, favoring detachment-limited models over purely transport-limited models. Erosion in the drawdown reach (Gardner, 1983) may explain rounding or steep gradients above lips in several profiles. In a compilation of knickpoint vertical relief (Figure DR1[1]), the tallest knickpoints occur within 11 km of the frontmost thrust. Knickpoints found landward of 11 km were much smaller (<100 m). Hence, knickpoints record concentration of tectonic activity around the front of the wedge.

MODELING KNICKPOINT EVOLUTION

A numerical model is presented here that furthers the investigation of the relative importance of advective and diffusive behavior in the

[1]GSA Data Repository item 2006065, Figures DR1: graph of knickpoint vertical relief versus distance from the tectonic range front and DR2: misfit graphs for models of Barbados prism channels, is available on the Web at http://www.geosociety.org/pubs/ft2006.htm. Requests may also be sent to editing@geosociety.org.

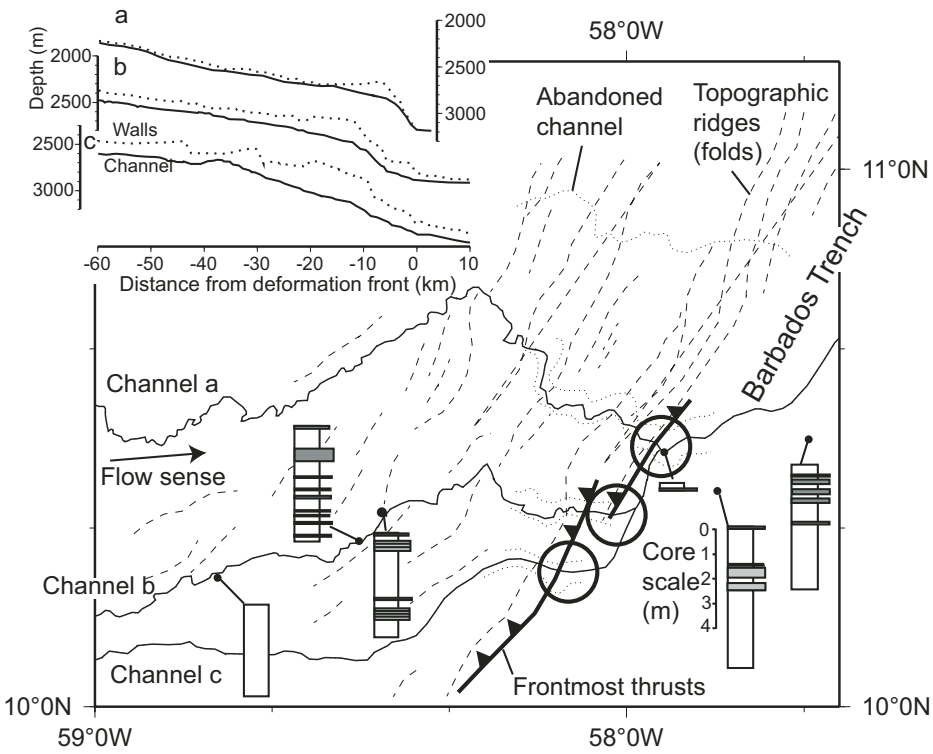

Figure 8. Physiography of the southern Barbados accretionary prism interpreted from a bathymetry image in Huyghe et al. (2004). Dashed lines mark the crests of ridges formed by thrust folds, and bold lines with barbs are the frontal thrusts interpreted by Huyghe et al. The lines of the profiles (inset) are marked with fine solid lines (channels) and dotted lines (adjacent canyon walls). Circles mark the frontmost thrusts that form the origin of the profiles. Also shown are schematic representations of core logs (Faugeres et al., 1993) (white and gray intervals represent fines and sandy sediments, respectively). Inset (top left) shows three channel profiles interpreted by Huyghe et al. from their multibeam data (continuous lines) and adjacent canyon wall topography (dotted lines).

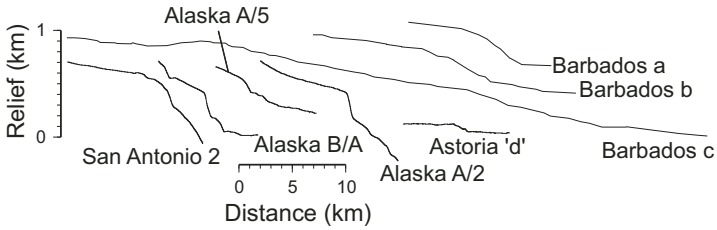

Figure 9. Compilation of knickpoint lip morphologies shown with equal 10:1 vertical exaggeration. The profiles were derived from lines 2 of Figure 7, d of Figure 6, 2 and 5 of Figure 4, A of Figure 5, and a, b, and c of Figure 8.

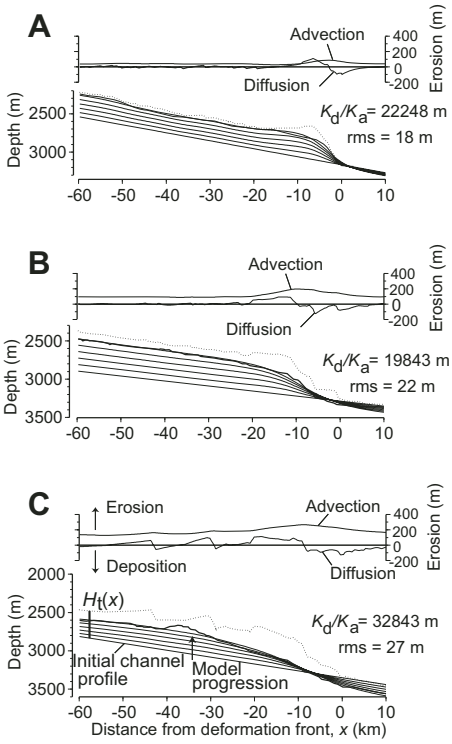

Figure 10. Relief of the three channels eroded through folds of the southern Barbados accretionary prism (Fig. 8) and best-fitting results of an erosion model (rms—root-mean-square). The lines represent the channel beds (bold continuous lines) and adjacent elevations (dotted lines) of the canyon walls. The distances from the range front shown were measured along each channel. Model evolution is shown with fine lines, progressing as indicated by the arrow in C from a linear ramp (initial channel profile). Graphs above each channel show the modeled advective and diffusive components of bed evolution, i.e., the evaluated integrals involving, respectively, K_a and K_d in equation 14.

Barbados channels, chosen for modeling because their knickpoints are the largest, so backwater effects are minimized, and the area has already been well characterized (Faugeres et al., 1993; Griboulard et al., 1998; Huyghe et al., 2004). The channel knickpoints are in a young phase, and there is less of the ambiguity of multiple knickpoints that has been observed in other data sets.

A number of simplifying assumptions were required. Huyghe et al. (2004) argued that the steepest channel topography at −10 km in Figure 10C is evidence that thrust movements can occur out of sequence. The simplest assumption is adopted, however, in which all excess topography landward of the frontmost thrust (x < 0 km) was generated linearly with time over a common period, T, while accepting that discrepancies could reflect irregular tectonic movements (similar results are recovered for all three canyons, so this effect is probably not significant). The spatial variation in the cumulative differential tectonic uplift is represented by the relief $H_t(x)$ above a trend drawn parallel to the channels away from the knickpoint (e.g., "Initial channel profile" in Fig. 10C). It was assumed that turbidity currents passed through the canyons at a quasi-steady rate over time, so that a continuous erosion model can be applied. Huyghe et al. (2004) interpreted the reverse channel gradient near −40 km in Figure 10C as implying that, whereas tectonic

deformation is ongoing, erosion can be reduced during sea-level highstands, as at present when sediment is mostly stored on the shelf, allowing tectonic activity to distort the profile. The period represented by syntectonic fans is around 1 m.y., based on their thicknesses and sedimentation time scales (Huyghe et al., 2004). Erosion therefore occurred over multiple glacial cycles and can be regarded as episodic, with a characteristic glacial period that is still much smaller than the total period over which deformation has built the anticlines; so erosion behavior can be approximated by steady erosion. A further assumption was that substrate erodibility is uniform laterally and in depth. Various fractures and associated diagenetic products observed by Griboulard et al. (1998) may have led to some heterogeneity. By analogy with Nankai Trough sediments (Bray and Karig, 1986; Screaton et al., 2002), progressively increasing shear strength with depth and a moderate induration is expected at the maximum 300 m eroded depth of the Barbados channels. Varied bed erodibility was not included, because it would add complexity without necessarily making the results more illuminating. Given these assumptions and further trade-offs between parameters described in the following, the results are nonunique and should not be read as providing accurate constraints on the erosion equation parameters.

The evolving channel topography was represented with an array of 100-m-spaced nodes, in which elevations were adjusted iteratively. The model initial condition was $H_0(x) = H_{0a} - H_{0b}x$, where x is the graph ordinate and H_{0a} and H_{0b} are the offset and gradient of the initial channel profile. In each time step Δt, the channel bed was elevated by $H_t\Delta t/T$, where $\Delta t/T = 1/10^5$ iterations and $H_t(x)$ is the present thrust-generated topography defined in Figure 10C. The channel bed was also eroded by an amount $K_a|\partial z/\partial x|^{2/3} + K_d\partial^2 z/\partial x^2$ (Rosenbloom and Anderson, 1994), where the gradient $\partial z/\partial x$ and curvature $\partial^2 z/\partial x^2$ were calculated from finite differences of the profile topography, and the term in $\partial z/\partial x$ applied only where $\partial z/\partial x$ was negative (downgradient). Thus, the model channel topography evolved according to:

$$z(x,t) = H_0(x) + H_t(x)\frac{t}{T} - \int_0^t \left(K_a \left|\frac{\partial z}{\partial x}\right|^{2/3} + K_d\left(\frac{\partial^2 z}{\partial x^2}\right)\right) dt \ . \quad (14)$$

Equations 7 and 12 were combined to represent erosion, because the profiles are smoother than the driving tectonic topography H_t in Figure 8 (inset), hence, by observation, they appear to have evolved diffusively as well as advectively. The origin of diffusion is unclear—the profiles may have become smooth because coarser sediment load filled depressions, temporarily preventing those areas from eroding, while intervening areas with typically negative $\partial^2 z/\partial x^2$ were exposed to erosion. Without detailed observations, it is difficult to say how both advection and diffusion arise, but equation 14 nevertheless appears to represent the channel topography well. The 2/3 power was applied to gradient (erosion rates proportional to bed shear stress; Howard and Kerby, 1983). Prescribing the exponent reduces the number of free parameters, and in practice it would be poorly resolved, because effects of varied n trade off with the diffusive term. The initial slope $H_0(x)$ and tectonic uplift $H_t(x)$ were extrapolated at constant gradient (H_{0b}) 50 km downstream and 10 km upstream of the domains of the profiles in Figure 10 to prevent errors associated with boundaries from affecting the domain of interest.

The model was repeated and parameters K_a and K_d were found by grid search, locating solutions with minimum root-mean-square (rms) difference between model and observed channel profiles (Figure DR2, see footnote one). As T was unknown, K_a and K_d were scaled to T, and their absolute values are not meaningful. Note also that K_a and K_d have different units, so their magnitudes are not comparable. However, the ratio K_d/K_a given beside each profile in Figure 10 can be compared between the profiles, to indicate variations in the relative importance of the diffusive and advective terms in equation 14. Their net (integrated) contributions are also shown by the erosion profiles above each graph. Considering those profiles and the K_d/K_a ratios, the relative importance of advection and diffusion varies little between the three channels.

Despite the smaller rms values, the solutions in Figures 10A and 10B are worse than that in Figure 10C at the knickpoint lips and bases. The latter error might be explained by hydraulic jumps of currents having led to localized erosion. Alternatively, localized erosion occurred because of fluids released along faults or was caused by pore water hydraulic gradients modified by the canyon topography (Orange and Breen, 1992). As mentioned earlier, the models are better compared against the knickpoint lip morphology.

To illustrate that neither diffusion nor advection alone represents the erosion well, Figure 11 shows best-fitting solutions with $K_a = 0$ for diffusion only (dashed lines) and with K_d made small (solid gray lines) for primarily advection conditions (retaining some diffusion for numerical stability). The diffusion-only graphs, though partially representing the rounding of knickpoint lips, are unable to reproduce convexity fully. The solutions with primarily advection mimic the tectonic topography, though with the center of the knickpoint face lying upstream relative to the center of the tectonic relief, as expected (Fig. 2B). However, such solutions tend not to represent rounding of the lip particularly well. The deficiencies in both methods compensate for each other, so that the combined equation represents the observed channel profiles well.

Alternatively, nondeposition or erosion at the base of the knickpoint slope caused by a hydraulic jump or pore fluid expulsion could explain the poor fit of the simple diffusion model. In Figure 12, the third set of model curves for each channel shows the result of imposing a sink in the transport flux at the base of slope (zero erosion or deposition boundary condition). Although profile shapes are not reproduced exactly (e.g., in Fig. 11A, a diffusion model cannot reproduce the flat topography in the reach above the lip and the sharp curvature of the lip itself), the predicted channel shapes nevertheless replicate the observed profiles relatively well (vertical separations can be simply ascribed to initial channel relief).

The models were also adapted to investigate effects of a threshold of erosion or bedload transport. Figure 12 reproduces the solutions of Figure 11B for diffusion-only (dashed lines in upper graph) and advection-only (gray lines in lower graph) conditions. The transport-limited model with a threshold gradient was represented by:

$$z(x,t) = H_0(x) + H_t(x)\frac{t}{T} - K_d\int_0^t \frac{\partial q}{\partial x}dt \ , \quad (15).$$

with $q = (|\partial z/\partial x| - S_0)$; $-\partial z/\partial x > S_0$ (i.e., flow downgradient). The solution is similar to Figure 2E, but the knickpoint face develops a linear ramp differently, because initially only a localized channel area is steeper than S_0, but it then broadens progressively with progressive tectonic steepening. Detachment-limited erosion with a threshold was simulated with:

$$z(x,t) = H_0(x) + H_t(x)\frac{t}{T} - K_a\int_0^t \left(\left|\frac{\partial z}{\partial x}\right|^{2/3} - S_0^{2/3}\right) dt \ , \quad (16)$$

where the term in brackets was evaluated using $-\partial z/\partial x > S_0$ (i.e., flow downgradient).

In both cases, the threshold sharpens the knickpoint lip, a tendency not observed in the actual channel profile. Unless fortuitously offset by increasing resistance to erosion with burial depth, the round lips imply that flow stress commonly exceeds thresholds here.

DISCUSSION

Although some knickpoints may have arisen during simple entrenchment because of lateral variations in erosional resistance, those in uniform turbidites are more difficult to explain by such mechanisms and are interpreted as having migrated upstream. Migration implies that erosion occurs where flows become more vigorous on steep gradients. A transport-limited scheme is then less likely than a detachment-limited scheme, although flow momentum effects also need to be considered when interpreting knickpoint shapes in detail. G. Parker (2005, personal commun.) described how eroded steps can migrate upstream associated with cyclic bed shear stress focused at the base of each step, a migration analogous to that of headcuts (Stein and Julien, 1993).

The various shapes of knickpoint lips may have arisen for one or more reasons. Rounding could arise from erosion associated with drawdown (Gardner, 1983), because the slope exponent in equation 9 is less than unity (Fig. 2B), because increasing induration or shear strength with burial depth leads to depth-increasing resistance (depth-increasing K_a), or because erosion may involve diffusive processes, as suggested for the Barbados channels. As mentioned, sharp lips are unlikely to have arisen from a resistant cap (Holland and Pickup, 1976), because shear strength typically increases with depth. More likely explanations involve a significant threshold of erosion compared with flow stresses (Fig. 2C) or flow separation over the lip, if it is particularly sharp (Stein and Julien, 1993).

The strong density stratification of turbidity currents can lead to different behavior compared with that expected from layer-averaged flow properties (Kneller and McCaffrey, 1999). As the weight and static pressure terms of equation 2 are dominated by the basal dense layer, the base may tend to accelerate faster than the broader, less dense upper section across a steepening gradient. The extent to which the base approaches equilibrium velocity faster than the upper flow depends on how momentum is transferred vertically, in particular the efficiency of eddies, which can reach dimensions of flow thickness (Kneller et al., 1999). Laboratory experiments are needed to explore how backwater length scales are affected.

Effect of a Threshold of Erosion or Transport

Simulations of river bed erosion illustrate that it is important to understand both how the shear stress of a typical flood exceeds threshold, and also the full size distribution of bed shear stress

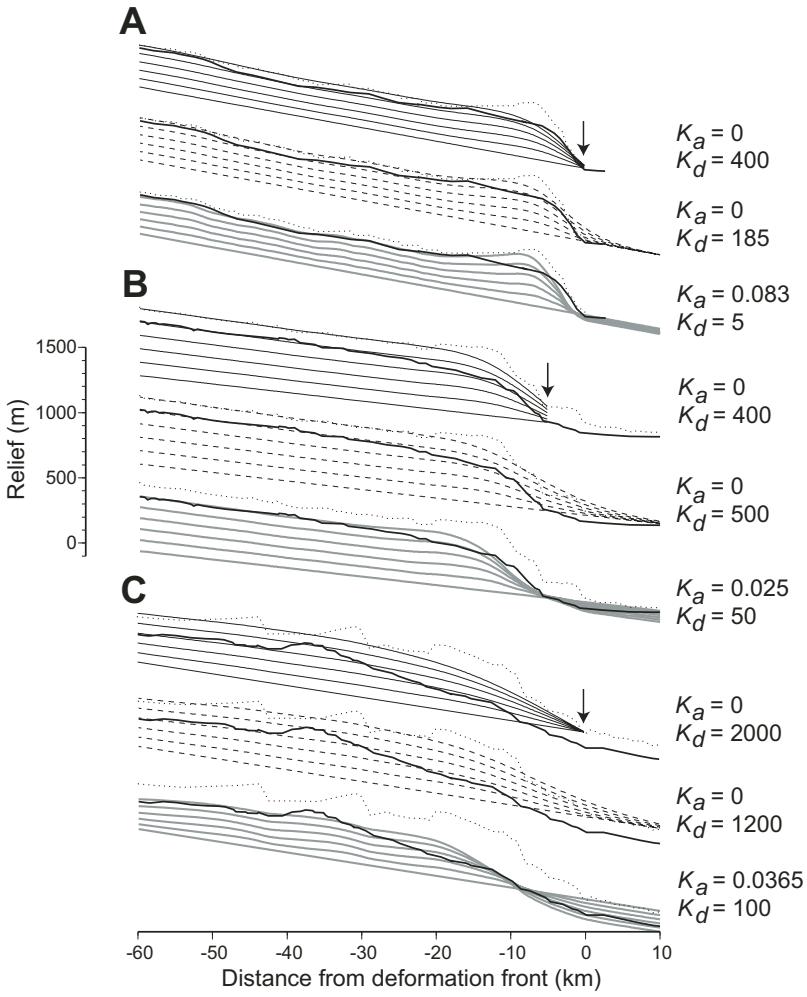

Figure 11. Erosion model solutions for the Barbados channels with only diffusion (dashed curves) and with advection and minor diffusion (bold gray curves) and for only diffusion with an imposed nondeposition/erosion boundary condition at the points marked by vertical arrows (thin gray curves). Values for the model parameters are shown on the right (units of K_a are m/iteration and of K_d are m²/iteration).

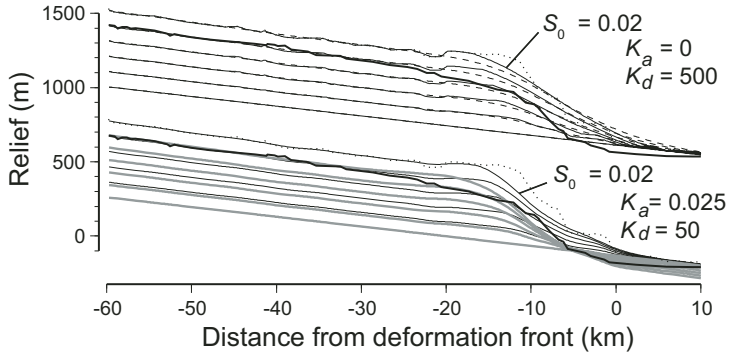

Figure 12. Effect of a threshold gradient for Barbados channel b. Dashed lines in the top graph reproduce the diffusion-only solution, and gray lines in the lower graph the advection-only solution of Figure 11. Fine solid lines show the result of imposing a threshold gradient of S_0 = 0.02 for erosion or bedload transport, in both cases sharpening the knickpoint lip more than is observed.

resulting from variability of rainfall and catchment hydrology (Snyder et al., 2003; Tucker, 2004; Tucker and Bras, 2000). A large flood may cause long reaches to exceed threshold and erode, whereas a lesser flood may erode more localized areas.

A rough comparison can be made between river discharge characteristics and turbidite sequences, which suggests that turbidity currents may be comparably varied. The ratio of peak to average discharge (Q_{flood}/Q_{av}) of rivers ranges from 10^0 to 10^4 (Mulder and Syvitski, 1995). Finnegan et al.'s (2005) model for widening of a stream with increasing discharge suggests (their equations 3 and 4) that the mean flow velocity $U \propto Q^{1/4}$ and thus $\tau_b \propto Q^{1/2}$. The range in Q_{flood}/Q_{av} implies a range of 10^0–10^2 in τ_{flood}/τ_{av} and of 10^0–10^1 in U_{flood}/U_{av}.

A strong variability of turbidity current stresses is suggested by turbidite bed thicknesses varying over two or more orders of magnitude in a given basin. In one study, thickness distributions for a Nevada field area and a forearc basin were almost power law over two orders of magnitude (Rothman et al., 1994), with fewer large beds than small beds, i.e., large flows were relatively infrequent, as is the case with river discharge. Thicker beds are associated with coarser basal sediment (Sadler, 1982; Talling, 2001). As the mean flow speed $\geq w/S$ (Komar, 1977) and unhindered settling velocity w (Gibbs et al., 1971) implied by Talling's grain-size data varies by one order of magnitude, velocities along transport paths can vary significantly between flows, although full interpretation requires knowledge of depositional geography (Bowen et al., 1984). Laboratory experiments have also revealed large shear stress variations associated with eddies within the current body (Kneller and Buckee, 2000).

The net effect of variability within and between flows could thus be as significant as for some rivers of strongly variable discharge, and comparable morphological consequences can be expected. As different thickness distributions have been reported for different areas (Talling, 2001), flow variability could vary between different canyons. The various shapes of knickpoint lips may, therefore, also reflect differences in flow stress variability relative to thresholds.

Role of the Turbidity Current Head

Erosion associated with turbulent tunnels and lobes beneath heads was originally considered to explain spacings of flute marks on the lower surfaces of turbidites (Allen, 1971). Knickpoint migration, however, is more consistent with the emerging view that turbidity currents supplying deep sedimentary fans are long-lived (Damuth et al., 1988), lasting hours to days based on flow reconstructions (Normark and Piper, 1991) and observations (Xu et al., 2004). This is because experiments have shown that the head's velocity varies only weakly with bed gradient (Middleton, 1966a). Erosion or transport rate associated with the head should therefore vary independently of bed gradient and would not obviously affect knickpoint morphology. This is indirect evidence that the body of the current, which has a velocity that responds to gradient, causes most of the erosion.

Comparing Submarine with Fluvial Erosion

The introduction herein outlined evidence for how erosion by turbidity currents could involve similar processes to fluvial erosion. As beds incised in submarine settings are often less indurated than bedrock in the fluvial examples, the correspondence of knickpoint morphology between the two environments is perhaps surprising, but the following suggests that some differences may yet emerge. The review given in the introduction suggests that removal of substrate material can occur in an analogous manner to rigid-block quarrying, plucking, and abrasion in bedrock rivers, leading to a similar dependence of erosion rate on flow speed. Scaling arguments (Hancock et al., 1998; Whipple et al., 2000) suggest that quarrying should lead to $E \propto S^{2/3}$, whereas abrasion leads to $E \propto S^{5/3}$. The latter involves a relation for how suspended sediment concentration rises with river flow velocity. There is a similar expectation that stronger turbidity currents carry heavier particles in suspension (Bagnold, 1963), so the abrasion dynamics may turn out to be similar.

The arguments for quarrying may translate to submarine beds composed of indurated rock without much difficulty, but the situation is complicated if the bed is cohesive sediment. An analogous argument to quarrying can be envisaged, in which bed shear stress imposed by the flow and uplift resulting from the flow's velocity cause shear failure. The quarrying argument involves flow shear stress working against frictional shear resistance stress along joints of a rigid block or flow-induced pressure reduction causing uplift opposed by the block's weight (Hancock et al., 1998). In cohesive sediment, the flow stress is opposed by the sediment's shear strength, or flow negative pressure causes uplift opposed by the sediment's weight but also opposed by sediment cohesion. In rivers, as deeply buried bedrock is exhumed, joints develop by stress relaxation and bed processes so that erosion can continue over the long time scales associated with mountain uplift and denudation (Whipple et al., 2000). However, because sediment shear strength typically increases with depth of original burial (Skempton, 1970), submarine bed erosion by shear failure is limited to depths where shear strength is less than stresses imposed by the flows (Mulder et al., 1998). In other words, unloading of cohesive sediment does not obviously reduce its shear strength in an analogous way to joint development in river beds. A possible exception to this is biological attack (Dillon and Zimmerman, 1970; Malahoff et al., 1982; Paull et al., 2005; Valentine et al., 1980; Warme et al., 1978) preparing the bed between flows, but its efficiency remains to be quantified. That canyon floors become more resistant to erosion with increasing exhumation is implied by U.S. Atlantic slope canyons (Mitchell, 2004, 2005), which have similar gradients at mid-slope despite a variety of contributing areas, suggesting a buffering of erosion. Because of its depth limitation, flow-induced shear failure may turn out be less important for excavating deep canyons than abrasion.

CONCLUSIONS

In submarine canyons, sharp changes of channel gradient are initiated by faults and anticlinal folds in convergent margins and in continental slopes affected by shale and salt tectonics, by deep entrenchment of main channels leaving tributaries as hanging valleys, and by breached levees in fan channels. The largest knickpoints studied here, from the southern Barbados accretionary prism, are rounded, as though affected by diffusion, but are also upstream of the trenchmost faults. A simple model using both advection and diffusion representing detachment- and transport-limited erosion represents the channel topography reasonably well, but diffusion alone can also adequately reproduce the data if a boundary condition (nondeposition/erosion representing sediment mobilized by a hydraulic jump or by pore fluid expulsion) is applied at the base of the slope. A threshold of erosion or transport would sharpen the lip, which is the opposite tendency to the rounding observed, so in this setting, threshold effects are minor or fortuitously compensated (e.g., by increasing sediment resistance with burial depth).

The other knickpoints studied, which are mostly shorter than backwater length scales, have a variety of forms. Lips vary from sharp to rounded. Although an origin by varied resistance to erosion is difficult to rule out for any individual knickpoint, several knickpoints lie within uniform turbidites with no obvious sign in the data of localized resistant lithology. Their locations upstream of steep topography therefore suggest that they have migrated, implying that enhanced flow velocity on gradients leads to enhanced ero-

sion and topographic advection. Migration is more consistent with erosion being carried out by the body of the current than the head, as the head velocity is unresponsive to bed gradient.

The variety of shapes of the lips could originate for various reasons. Rounding could arise because of erosion associated with drawdown; erosion rate is related to gradient with a small power-law exponent, because of increasing induration or shear strength with depth, because of varied component of bedload transport, or because sediment accumulates in depressions, which protects them while protrusions (areas of negative curvature) are eroded. Sharp lips may arise from a significant threshold of erosion relative to flow-imposed shear stresses. The strong variability of thickness and grain size of turbidite sequences suggests that the range of shear stress imposed by turbidity currents could be comparable to those imposed by some rivers of strongly varied discharge. Shear stress variability could vary between different channels, providing a further explanation for the variety of knickpoint forms.

The processes of quarrying and abrasion of bedrock are likely to be similar to those occurring in rivers. Shear failure of consolidated sediment, however, should be limited to the depth at which the flow can overcome shear strength and hence erosion is buffered, unless the bed can be prepared between flows by biological or other processes.

ACKNOWLEDGMENTS

Some of this work was supported by a research fellowship from the Royal Society [London]. The Alaska, Chile, Oregon, and New Jersey slope data were provided by the National Geophysical Data Center (NGDC, www.ngdc.noaa.gov). Thanks are due to the scientists and crews of the marine surveys collecting these data. Gary Parker and Binliang Lin provided valuable advice on backwater length scales. Jim Gardner and two anonymous reviewers helpfully commented on an earlier version of this work. Greg Tucker, Kelin Whipple, and Ellen Wohl are thanked for helpful detailed comments, which significantly improved the paper. The idea of looking at knickpoints was first suggested to me by Brian Dade, and Niels Hovius pointed out the importance of changes in flow width. The Figures were created with the Generic Mapping Tools software (Wessel and Smith, 1991).

REFERENCES CITED

Adeogba, A.A., McHargue, T.R., and Graham, S.A., 2005, Transient fan architecture and depositional controls from near-surface 3-D seismic data, Niger Delta continental slope: American Association of Petroleum Geology Bulletin, v. 89, p. 627–643.

Allen, J.R.L., 1971, Mixing at turbidity current heads, and its geological implications: Journal of Sedimentary Petrology, v. 41, p. 97–113.

Altinakar, M.S., Graf, W.H., and Hopfinger, E.J., 1996, Flow structure in turbidity currents: Journal of Hydraulic Research, v. 34, p. 713–718.

Bagnold, R.A., 1963, Mechanics of marine sedimentation, *in* Hill, M.N., ed., The sea, Volume 3: New York, Wiley, p. 507–528.

Begin, Z.B., 1988, Application of a diffusion-erosion model to alluvial channels which degrade due to base-level lowering: Earth Surface Processes and Landforms, v. 13, p. 487–500.

Begin, Z.B., Meyer, D.F., and Schumm, S.A., 1981, Development of longitudinal profiles of alluvial channels in response to base-level lowering: Earth Surface Processes and Landforms, v. 6, p. 49–68.

Belderson, R.H., Kenyon, N.H., Stride, A.H., and Pelton, C.D., 1984, A "braided" distributary system on the Orinoco deep-sea fan: Marine Geology, v. 56, p. 195–206, doi: 10.1016/0025-3227(84)90013-6.

Bishop, P., and Goldrick, G., 1992, Morphology, processes and evolution of two waterfalls near Cowra, New South Wales: The Australian Geographer, v. 23, p. 116–121.

Bowen, A.J., Normark, W.R., and Piper, D.J.W., 1984, Modelling of turbidity currents on Navy Submarine Fan, California continental borderland: Sedimentology, v. 31, p. 169–185.

Bray, C.J., and Karig, D.E., 1986, Physical properties of sediments from the Nankai Trough, Deep Sea Drilling Project Leg 87A, Sites 582 and 583, *in* Kagami, H., Karig, D.E., Coulbourn, W.T., et al., Initial Reports of the Deep Sea Drilling Project Volume 87: Washington, D.C., U.S. Government Printing Office, p. 827–842.

Bruns, T.R., 1985, Tectonics of the Yakutat block, an allochthonous terrane in the northern Gulf of Alaska: U.S. Geological Survey Open-File Report 85-13, 112 p.

Burbank, D.W., and Anderson, R.S., 2001, Tectonic geomorphology: Malden, Massachusetts, Blackwell, 288 p.

Carlson, P.R., and Nelson, C.H., 1987, Marine geology and resource potential of the Cascadia Basin, *in* Scholl, D.W., et al., eds., Geology and resource potential of the continental margin of western North America and adjacent ocean basins—Beaufort Sea to Baja California: Houston, Texas, Circum-Pacific Council for Energy and Mineral Resources, p. 523–535.

Chikita, K., 1990, Sedimentation by river-induced turbidity currents: Field measurements and interpretation: Sedimentology, v. 37, p. 891–905.

Cui, Y., Parker, G., Lisle, T.E., Gott, J., Hansler, M.E., Pizzuto, J.E., Allmendinger, N.E., and Reed, J.M., 2003, Sediment pulses in mountain rivers, I. Experiments: Water Resources Research, v. 39, paper 1239, doi: 10.1029/2002WR001803.

Dade, W.B., and Friend, P.F., 1998, Grain-size, sediment-transport regime, and channel slope in alluvial rivers: The Journal of Geology, v. 106, p. 661–675.

Daly, R.A., 1936, Origin of submarine "canyons": American Journal of Science, v. 231, p. 401–420.

Damgaard, J., Soulsby, R., Peet, A., and Wright, S., 2003, Sand transport on steeply sloping plane and ripple beds: Journal of Hydraulic Engineering, v. 129, p. 706–719, doi: 10.1061/(ASCE)0733–9429(2003)129.:9(706).

Damuth, J.E., Flood, R.D., Kowsmann, R.O., Belderson, R.H., and Gorini, M.A., 1988, Anatomy and growth pattern of Amazon deep-sea fan as revealed by long-range side-scan sonar (GLORIA) and high-resolution seismic studies: American Association of Petroleum Geology Bulletin, v. 72, p. 885–911.

de Moustier, C., and Kleinrock, M.C., 1986, Bathymetric artifacts in Sea Beam data: How to recognize them and what causes them: Journal of Geophysical Research, v. 91, p. 3407–3424.

Dillon, W.P., and Zimmerman, H.B., 1970, Erosion by biological activity in two New England submarine canyons: Journal of Sedimentary Petrology, v. 40, p. 542–547.

Duvall, A., Kirby, E., and Burbank, D., 2004, Tectonic and lithologic controls on bedrock channel profiles and processes in coastal California: Journal of Geophysical Research, v. 109, p. F03002, doi: 10.1029/2003JF000086.

Farre, J.A., 1987, Surficial geology of the continental margin offshore New Jersey in the vicinity of Deep Sea Drilling Project Sites 612 and 613, *in* Poag, C.W., and Watts, A.B., eds., Initial Reports Deep Sea Drilling Project, Volume 95: Washington, D.C., U.S. Government Printing Office, p. 725–759.

Farre, J.A., and Ryan, W.B.F., 1985, 3-D view of erosional scars on U.S. mid-Atlantic continental margin: American Association of Petroleum Geologists Bulletin, v. 69, p. 923–932.

Farre, J.A., McGregor, B.A., Ryan, W.B.F., and Robb, J.M., 1983, Breaching the shelfbreak: Passage from youthful to mature phase in submarine canyon evolution, *in* Stanley, D.J., and Moore, G.T., eds., The shelfbreak: Critical interface on continental margins: Society of Economic Paleontologists and Mineralogists Special Publication 33, p. 25–39.

Faugeres, J.C., Gonthier, E., Griboulard, R., and Masse, L., 1993, Quaternary sandy deposits and canyons on the Venezuelan margin and south Barbados accretionary prism: Marine Geology, v. 110, p. 115–142, doi: 10.1016/0025-3227(93)90109-9.

Finnegan, N.J., Roe, G., Montgomery, D.R., and Hallet, B., 2005, Controls on the channel width of rivers: Implications for modeling fluvial incision of bedrock: Geology, v. 33, p. 229–232, doi: 10.1130/G21171.1.

Foster, G.R., and Meyer, L.D., 1975, Mathematical simulation of upland erosion by fundamental erosion mechanics: Present and prospective technology for predicting sediment yields and sources (Proceedings of the 1972 Sediment Yield Workshop USDA-ARS, ARS-S40): Oxford, Mississippi, Agricultural Research Service, U.S. Department of Agriculture Sedimentation Lab, p. 190–207.

Fruehn, J., von Huene, R., and Fisher, M.A., 1999, Accretion in the wake of terrane collision: The Neogene accretionary wedge off Kenai Peninsula, Alaska: Tectonics, v. 18, p. 263–277, doi: 10.1029/1998TC900021.

Fukushima, Y., Parker, G., and Pantin, H.M., 1985, Prediction of ignitive turbidity currents in Scripps Submarine Canyon: Marine Geology, v. 67, p. 55–81, doi: 10.1016/0025-3227(85)90148-3.

Garcia, M.H., 1993, Hydraulic jumps in sediment-driven bottom currents: Journal of Hydraulic Engineering, v. 119, p. 1094–1117.

Garcia, M.H., and Parker, G., 1989, Experiments on hydraulic jumps in turbidity currents near a canyon-fan transition: Science, v. 245, p. 393–396.

Gardner, T.W., 1983, Experimental study of knickpoint migration and longitudinal profile evolution in cohesive homogeneous material: Geological Society of America Bulletin, v. 94, p. 664–672, doi: 10.1130/0016-7606(1983)94<664:ESOKAL>2.0.CO;2.

Gee, M.J.R., Masson, D.G., Watts, A.B., and Mitchell, N.C., 2001, Passage of debris flows and turbidity currents through a topographic constriction: Seafloor erosion and deflection of flow pathways: Sedimentology, v. 48, p. 1389–1409, doi: 10.1046/j.1365-3091.2001.00427.x.

Gibbs, R.J., Matthews, M.D., and Link, D.A., 1971, The relationships between sphere size and settling velocity: Journal of Sedimentary Petrology, v. 41, p. 7–18.

Goff, J.A., and Kleinrock, M.C., 1991, Quantitative comparison of bathymetric survey systems: Geophysical Research Letters, v. 18, p. 1253–1256.

Gray, T.A., Alexander, J., and Leeder, M.R., 2006, Quantifying velocity and turbulence structure in depositing sustained turbidity currents across breaks in slope: Sedimentology, v. 52, p. 467–488.

Griboulard, R., Bobier, C., Faugeres, J.C., Huyghe, P., Gonthier, E., Odonne, F., and Welsh, R., 1998, Recent tectonic activity in the South Barbados prism: Deep-towed side-scan sonar imagery: Tectonophysics, v. 284, p. 79–99, doi: 10.1016/S0040-1951(97)00164-9.

Hagen, R.A., Vergara, H., and Naar, D.F., 1996, Morphology of San Antonio submarine canyon on the central Chile forearc: Marine Geology, v. 129, p. 197–205, doi: 10.1016/0025-3227(96)83345-7.

Hancock, G.S., Anderson, R.S., and Whipple, K.X, 1998, Beyond power: Bedrock river incision process and form, *in* Tinkler, K.J., and Wohl, E.E., eds., Rivers over rock: Fluvial processes in bedrock channels: Washington, D.C., American Geophysical Union, p. 35–60.

Hanks, T.C., Bucknam, R.C., Lajoie, K.R., and Wallace, R.E., 1984, Modification of wave-cut and fault-controlled landforms: Journal of Geophysical Research, v. 89, p. 5771–5790.

Harbor, D.J., 1998, Dynamic equilibrium between an active uplift and the Sevier River, Utah: The Journal of Geology, v. 106, p. 181–194.

Holland, W.N., and Pickup, G., 1976, Flume study of knickpoint development in stratified sediment: Geological

Society of America Bulletin, v. 87, p. 76–82, doi: 10.1130/0016-7606(1976)87<76:FSOKDI>2.0.CO;2.
Howard, A.D., 1994, A detachment-limited model of drainage basin evolution: Water Resources Research, v. 30, p. 2261–2285, doi: 10.1029/94WR00757.
Howard, A.D., and Kerby, G., 1983, Channel changes in badlands: Geological Society of America Bulletin, v. 94, p. 739–752, doi: 10.1130/0016-7606(1983)94<739:CCIB>2.0.CO;2.
Hughes Clarke, J.E., Shor, A.N., Piper, D.J.W., and Mayer, L.A., 1990, Large-scale current-induced erosion and deposition in the path of the 1929 Grand Banks turbidity current: Sedimentology, v. 37, p. 613–629.
Hughes Clarke, J.E., Mayer, L.A., and Wells, D.E., 1996, Shallow-water imaging multibeam sonars: A new tool for investigating seafloor processes in the coastal zone and on the continental shelf: Marine Geophysical Researches, v. 18, p. 607–629, doi: 10.1007/BF00313877.
Huyghe, P., Foata, M., Deville, E., and Caramba Working Group, 2004, Channel profiles through the active thrust front of the southern Barbados prism: Geology, v. 32, p. 429–432.
Klaucke, I., and Cochonat, P., 1999, Analysis of past seafloor failures on the continental slope off Nice (SE France): Geo-Marine Letters, v. 19, p. 245–253, doi: 10.1007/s003670050115.
Klaucke, I., Savoye, B., and Cochonat, P., 2000, Patterns and processes of sediment dispersal on the continental slope off Nice: SE France: Marine Geology, v. 162, p. 405–422, doi: 10.1016/S0025-3227(99)00063-8.
Kneller, B., 1995, Beyond the turbidite paradigm: Physical models for deposition of turbidites and their implications for reservoir prediction, *in* Hartley, A.J., and Prosser, D.J., eds., Characterization of deep marine clastic systems: Geological Society [London] Special Publication 94, p. 31–49.
Kneller, B., and Buckee, C., 2000, The structure and fluid mechanics of turbidity currents: A review of some recent studies and their geological implications: Sedimentology, v. 47, p. 62–94, doi: 10.1046/j.1365-3091.2000.047s1062.x.
Kneller, B., and McCaffrey, W., 1999, Depositional effects of flow nonuniformity and stratification within turbidity currents approaching a bounding slope: Deflection, reflection, and facies variation: Journal of Sedimentary Petrology, v. 69, p. 980–991.
Kneller, B.C., Bennett, S.J., and McCaffrey, W.D., 1999, Velocity structure, turbulence and fluid stresses in experimental gravity currents: Journal of Geophysical Research, v. 104, no. C3, p. 5381–5391.
Komar, P.D., 1969, The channelized flow of turbidity currents with applications to Monterey deep-sea fan channel: Journal of Geophysical Research, v. 74, p. 4544–4558.
Komar, P.D., 1971, Hydraulic jumps in turbidity currents: Geological Society of America Bulletin, v. 82, p. 1477–1488.
Komar, P.D., 1977, Computer simulation of turbidity current flow and the study of deep-sea channels and fan sedimentation, *in* Goldberg, E.D., McCave, I.N., O'Brien, J.J., and Steele, J.H., eds., The sea: Ideas and observations on progress in the study of the seas: New York, John Wiley and Sons, p. 603–621.
Kukowski, N., Schillhorn, T., Huhn, K., von Rad, U., Husen, R., and Flueh, E.R., 2001, Morphotectonics and mechanics of the central Makran accretionary wedge off Pakistan: Marine Geology, v. 173, p. 1–19, doi: 10.1016/S0025-3227(00)00167-5.
Lavé, J., and Avouac, J.P., 2001, Fluvial incision and tectonic uplift across the Himalayas of central Nepal: Journal of Geophysical Research, v. 106, p. 26,561–26,591, doi: 10.1029/2001JB000359.
Lee, S.E., Talling, P.J., Ernst, G.G.J., and Hogg, A.J., 2002, Occurrence and origin of submarine plunge pools at the base of the US continental slope: Marine Geology, v. 185, p. 363–377, doi: 10.1016/S0025-3227(01)00298-5.
Lisle, T.E., Pizzuto, J.E., Ikeda, H., and Iseya, F., 1997, Evolution of a sediment wave in an experimental channel: Water Resources Research, v. 33, p. 1971–1981, doi: 10.1029/97WR01180.
Malahoff, A., Embley, R.W., and Fornari, D.J., 1982, Geomorphology of Norfolk and Washington Canyons and the surrounding continental slope and upper rise as observed with DSRV *Alvin*, *in* Scrutton, R.A., and Talwani, M., eds., The ocean floor: New York, John Wiley and Sons, p. 97–111.
Malinverno, A., Ryan, W.B.F., Auffret, G.A., and Pautot, G., 1988, Sonar images of recent failure events on the continental margin off Nice, France, *in* Clifton, H.E., ed., Sedimentological consequences of convulsive geologic events: Geological Society of America Special Paper 229, p. 59–75.
McAdoo, B.G., Orange, D.L., Screaton, E., Lee, H., and Kayen, R., 1997, Slope basins, headless canyons, and submarine palaeoseismology of the Cascadia accretionary complex: Basin Research, v. 9, p. 313–324, doi: 10.1046/j.1365-2117.1997.00049.x.
McAdoo, B.G., Pratson, L.F., and Orange, D.L., 2000, Submarine landslide geomorphology, US continental slope: Marine Geology, v. 169, p. 103–136, doi: 10.1016/S0025-3227(00)00050-5.
McGregor, B.A., Stubblefield, W.L., Ryan, W.B.F., and Twichell, D.C., 1982, Wilmington submarine canyon: A marine fluvial-like system: Geology, v. 10, p. 27–30, doi: 10.1130/0091-7613(1982)10<27:WSCAMF>2.0.CO;2.
McHugh, C.M., Ryan, W.B.F., and Schreiber, B.C., 1993, The role of diagenesis in exfoliation of submarine canyons: American Association of Petroleum Geologists Bulletin, v. 77, p. 145–172.
McNeill, L.C., Goldfinger, C., Kulm, L.D., and Yeats, R.S., 2000, Tectonics of the Neogene Cascadia forearc basin: Investigations of a deformed late Miocene unconformity: Geological Society of America Bulletin, v. 112, p. 1209–1224, doi: 10.1130/0016-7606(2000)112<1209:TOTNCF>2.3.CO;2.
Middleton, G.V., 1966a, Experiments on density and turbidity currents, I: Motion of the head: Canadian Journal of Earth Sciences, v. 3, p. 523–546.
Middleton, G.V., 1966b, Experiments on density and turbidity currents, II: Uniform flow of density currents: Canadian Journal of Earth Sciences, v. 3, p. 627–637.
Miller, J.R., 1991, The influence of bedrock geology on knickpoint development and channel-bed degradation along downcutting streams in south-central Indiana: The Journal of Geology, v. 99, p. 591–605.
Mitchell, N.C., 1996, Creep in pelagic sediments and potential for morphologic dating of marine fault scarps: Geophysical Research Letters, v. 23, no. 5, p. 483–486, doi: 10.1029/96GL00421.
Mitchell, N.C., 2004, Form of submarine erosion from confluences in Atlantic USA continental slope canyons: American Journal of Science, v. 304, p. 590–611.
Mitchell, N.C., 2005, Interpreting long-profiles of canyons in the USA Atlantic continental slope: Marine Geology, v. 214, p. 75–99, doi: 10.1016/j.margeo.2004.09.005.
Mitchell, N.C., Tivey, M.A., and Gente, P., 2000, Slopes of mid-ocean ridge fault scarps from submersible observations: Earth and Planetary Science Letters, v. 183, p. 543–555, doi: 10.1016/S0012-821X(00)00270-3.
Mohrig, D., and Marr, J.G., 2003, Constraining the efficiency of turbidity current generation from submarine debris flows and slides using laboratory experiments: Marine and Petroleum Geology, v. 20, p. 883–899, doi: 10.1016/j.marpetgeo.2003.03.002.
Mulder, T., and Syvitski, J.P.M., 1995, Turbidity currents generated at river mouths during exceptional discharges to the world's oceans: The Journal of Geology, v. 103, p. 285–299.
Mulder, T., Syvitski, J., and Skene, K., 1998, Modeling of erosion and deposition by turbidity currents generated at river mouths: Journal of Sedimentary Research, v. 68, p. 124–137.
Mulder, T., Cirac, P., Gaudin, M., Bourillet, J.-F., Tranier, J., Normand, A., Weber, O., Griboulard, R., Jouanneau, J.-M., Anschutz, P., and Jorissen, F.J., 2004, Understanding continent-ocean sediment transfer: Eos (Transactions, American Geophysical Union), v. 85, p. 257–262.
Nelson, C.H., 1976, Late Pleistocene and Holocene depositional trends, processes, and history of Astoria deep-sea fan, northeast Pacific: Marine Geology, v. 20, p. 129–173, doi: 10.1016/0025-3227(76)90083-9.
Normark, W.R., 1989, Observed parameters for turbidity-current flow in channels, Reserve Fan, Lake Superior: Journal of Sedimentary Petrology, v. 59, p. 423–431.
Normark, W.R., and Piper, D.J.W., 1991, Initiation processes and flow evolution of turbidity currents: Implications for the depositional record, *in* Osborne, R.H., ed., From shoreline to abyss: Tulsa, Oklahoma, Society of Economic Paleontologists and Mineralogists Special Publication 46, p. 207–230.
O'Connell, S., Normark, W.R., Ryan, W.B.F., and Kenyon, N.H., 1991, An entrenched thalweg channel on the Rhone Fan: Interpretation from a SeaBeam and SeaMARC I survey, *in* Osborne, R.H., ed., From shoreline to abyss: Tulsa, Oklahoma, Society of Economic Paleontologists and Mineralogists Special Publication 46, p. 259–270.
Orange, D.L., and Breen, N.A., 1992, The effects of fluid escape in accretionary wedges, II: Seepage force, slope failure, headless submarine canyons and vents: Journal of Geophysical Research, v. 97, p. 9277–9295.
Orpin, A.R., 2004, Holocene sediment deposition on the Poverty-slope margin by the muddy Waipaoa River: East coast New Zealand: Marine Geology, v. 209, p. 69–90.
Ouchi, S., 1985, Response of alluvial rivers to slow active tectonic movement: Geological Society of America Bulletin, v. 96, p. 504–515, doi: 10.1130/0016-7606(1985)96<504:ROARTS>2.0.CO;2.
Pantin, H.M., 1979, Interaction between velocity and effective density in turbidity flow: Phase-plane analysis, with criteria for autosuspension: Marine Geology, v. 31, p. 59–99, doi: 10.1016/0025-3227(79)90057-4.
Paola, C., 2000, Quantitative models in sedimentary basin filling: Sedimentology, v. 47, p. 121–178, doi: 10.1046/j.1365-3091.2000.00006.x.
Parker, G., Fukushima, Y., and Pantin, H.M., 1986, Self-accelerating turbidity currents: Journal of Fluid Mechanics, v. 171, p. 145–181.
Paull, C.K., Ussler, W., Greene, H.G., Barry, J., and Keaten, R., 2005, Bioerosion by chemosynthetic biological communities on Holocene submarine slide scars: Geo-Marine Letters, v. 25, p. 11–19.
Peakall, J., McCaffrey, W., and Kneller, B., 2000, A process model for the evolution, morphology, and architecture of sinuous submarine channels: Journal of Sedimentary Research, v. 70, p. 434–448.
Piper, D.J.W., Shor, A.N., Farre, J.A., O'Connell, S., and Jacobi, R., 1985, Sediment slides and turbidity currents on the Laurentian Fan: Sidescan sonar investigations near the epicenter of the 1929 Grand Banks earthquake: Geology, v. 13, p. 538–541, doi: 10.1130/0091-7613(1985)13<538:SSATCO>2.0.CO;2.
Piper, D.J.W., Shor, A.N., and Hughes Clarke, J.E., 1988, The 1929 "Grand Banks" earthquake, slump and turbidity current, *in* Clifton, H.E., ed., Sedimentological consequences of convulsive geologic events: Geological Society of America Special Paper 229, p. 77–92.
Piper, D.J.W., Cochonat, P., and Morrison, M.L., 1999, The sequence of events around the epicentre of the 1929 Grand Banks earthquake: Initiation of debris flows and turbidity current inferred from sidescan sonar: Sedimentology, v. 46, p. 79–97, doi: 10.1046/j.1365-3091.1999.00204.x.
Pirmez, C., and Imran, J., 2003, Reconstruction of turbidity currents in Amazon Channel: Marine and Petroleum Geology, v. 20, p. 823–849, doi: 10.1016/j.marpetgeo.2003.03.005.
Pirmez, C., Pratson, L.F., and Steckler, M.S., 1998, Clinoform development by advection-diffusion of suspended sediment: Modeling and comparison to natural systems: Journal of Geophysical Research, v. 103, p. 24,141–24,157, doi: 10.1029/98JB01516.
Pirmez, C., Beaubouef, R.T., Friedmann, S.J., and Mohrig, D.C., 2000, Equilibrium profile and baselevel in submarine channels: Examples from late Pleistocene systems and implications for the architecture of deepwater reservoirs, *in* Weimer, P., et al., eds., Deepwater reservoirs of the world: Gulf Coast Section, Society of Economic Paleontology and Mineralogy Foundation 20th Annual Research Conference, p. 782–805.
Plafker, G., 1987, Regional geology and petroleum potential of the northern Gulf of Alaska continental margin, *in* Scholl, D.W., Grantz, A., and Vedder, J.G., eds., Geology and resource potential of the continental margin of western North America and adjacent ocean basins—Beaufort Sea to Baja California: Houston, Texas, Circum-Pacific Council for Energy and Mineral Resources, p. 229–268.
Popescu, I., Lericolais, G., Panin, N., Normand, A., Dinu, C., and Le Drezen, E., 2004, The Danube submarine

canyon (Black Sea): Morphology and sedimentary processes: Marine Geology, v. 206, p. 249–265, doi: 10.1016/j.margeo.2004.03.003.

Prather, B.E., 2003, Controls on reservoir distribution, architecture and stratigraphic trapping in slope settings: Marine and Petroleum Geology, v. 20, p. 529–545, doi: 10.1016/j.marpetgeo.2003.03.009.

Pratson, L.F., and Ryan, W.B.F., 1996, Automated drainage extraction for mapping the Monterey submarine drainage system, California margin: Marine Geophysical Researches, v. 18, p. 757–777, doi: 10.1007/BF00313885.

Pratson, L.F., Imran, J., Parker, G., Syvitski, J.P.M., and Hutton, E.W.H., 2000, Debris flows versus turbidity currents: A modeling comparison of their dynamics and deposits, *in* Bouma, A., et al., eds., Fine-grained turbidite systems: Tulsa, Oklahoma, Society of Economic Paleontologists and Mineralogists, p. 57–71.

Robb, J.M., 1984, Sapping on the lower continental slope, offshore New Jersey: Geology, v. 12, p. 278–282, doi: 10.1130/0091-7613(1984)12<278:SSOTLC>2.0.CO;2.

Robb, J.M., Hampson, J.C., Kirby, J.R., and Twichell, D.C., 1981, Geology and potential hazards of the continental slope between Lindenkohl and South Toms Canyons, offshore Mid-Atlantic United States: U.S. Geological Survey Open-File Report 81-600, 33 p.

Robb, J.M., Kirby, J.R., Hampson, J.C., Gibson, P.R., and Hecker, B., 1983, Furrowed outcrops of Eocene chalk on the lower continental slope offshore New Jersey: Geology, v. 11, p. 182–186, doi: 10.1130/0091-7613(1983)11<182:FOOECO>2.0.CO;2.

Rosenbloom, N.A., and Anderson, R.S., 1994, Evolution of the marine terraced landscape, Santa Cruz, California: Journal of Geophysical Research, v. 99, p. 14,013–14,030, doi: 10.1029/94JB00048.

Rothman, D.H., Grotzinger, J.P., and Flemings, P., 1994, Scaling in turbidite deposition: Journal of Sedimentary Research, v. A64, no. 1, p. 59–67.

Ryan, W.B.F., 1982, Imaging of submarine landslides with wide-swath sonar, *in* Saxov, S., and Nieuwenhuis, J.K., eds., Marine slides and other mass movements (NATO Conference Series, vol. 6): New York, Plenum Press, p. 175–188.

Sadler, P.M., 1982, Bed-thickness and grain size in turbidites: Sedimentology, v. 29, p. 37–51.

Screaton, E., Saffer, D., Henry, P., Hunze, S., and Leg 190 Shipboard Scientific Party, 2002, Porosity loss within the underthrust sediments of the Nankai accretionary complex: Implications for overpressures: Geology, v. 30, p. 19–22.

Seidl, M.A., Dietrich, W.E., and Kirchner, J.W., 1994, Longitudinal profile development into bedrock: An analysis of Hawaiian channels: The Journal of Geology, v. 102, p. 457–474.

Shepard, F.P., 1981, Submarine canyons: Multiple causes and long-time persistence: American Association of Petroleum Geologists Bulletin, v. 65, p. 1062–1077.

Shipley, T.H., Stoffa, P.L., and Dean, D.F., 1990, Underthrust sediments, fluid migration paths, and mud volcanoes associated with the accretionary wedge off Costa Rica: Middle America Trench: Journal of Geophysical Research, v. 95, p. 8743–8752.

Shor, A.N., Piper, D.J.W., Hughes Clarke, J.E., and Mayer, L.A., 1990, Giant flute-like scour and other erosional features formed by the 1929 Grand Banks turbidity current: Sedimentology, v. 37, p. 631–645.

Skempton, A.W., 1970, The consolidation of clays by gravitational compaction: Journal of the Geological Society of London, v. 125, p. 373–411.

Skene, K., Mulder, T., and Syvitski, J.P.M., 1997, INFLO1: A model predicting the behaviour of turbidity currents generated at a river mouth: Computers & Geosciences, v. 23, p. 975–991, doi: 10.1016/S0098-3004(97)00064-2.

Sklar, L.S., and Dietrich, W.E., 2001, Sediment and rock strength controls on river incision into bedrock: Geology, v. 29, p. 1087–1090, doi: 10.1130/0091-7613(2001)029<1087:SARSCO>2.0.CO;2.

Smith, W.H.F., and Wessel, P., 1990, Gridding with continuous curvature splines in tension: Geophysics, v. 55, no. 3, p. 293–305, doi: 10.1190/1.1442837.

Snyder, N.P., Whipple, K.X, Tucker, G.E., and Merritts, D.J., 2003, Importance of stochastic distribution of floods and erosion thresholds in the bedrock river incision problem: Journal of Geophysical Research, v. 108, p. ETG17-1–ETG17-15, doi: 10.1029/2001JB001655.

Soh, W., and Tokuyama, H., 2002, Rejuvenation of submarine canyon associated with ridge subduction, Tenryu Canyon, off Tokai, central Japan: Marine Geology, v. 187, p. 203–230, doi: 10.1016/S0025-3227(02)00267-0.

Soulsby, R., 1997, Dynamics of marine sands, a manual for practical applications: London, Thomas Telford, 249 p.

Stacey, M.W., and Bowen, A.J., 1988, The vertical structure of density and turbidity currents: Theory and observation: Journal of Geophysical Research, v. 93, p. 3528–3542.

Steckler, M.S., Mountain, G.S., Miller, K.G., and Christie-Blick, N., 1999, Reconstruction of Tertiary progradation and clinoform development on the New Jersey passive margin by 2-D backstripping: Marine Geology, v. 154, p. 399–420, doi: 10.1016/S0025-3227(98)00126-1.

Stein, O.R., and Julien, P.Y., 1993, Criterion delineating the mode of headcut migration: Journal of Hydraulic Engineering (American Society of Civil Engineering), v. 119, p. 37–50.

Stock, J.D., and Montgomery, D.R., 1999, Geologic constraints on bedrock river incision using the stream power-law: Journal of Geophysical Research, v. 104, p. 4983–4993, doi: 10.1029/98JB02139.

Talling, P.J., 2001, On the frequency distribution of turbidite thickness: Sedimentology, v. 48, p. 1297–1329, doi: 10.1046/j.1365-3091.2001.00423.x.

Tucker, G.E., 2004, Drainage basin sensitivity to tectonic and climatic forcing: Implications of a stochastic model for the role of entrainment and erosion thresholds: Earth Surface Processes and Landforms, v. 29, p. 185–205, doi: 10.1002/esp.1020.

Tucker, G.E., and Bras, R.L., 2000, A stochastic approach in modeling the role of rainfall variability in drainage basin evolution: Water Resources Research, v. 36, p. 1953–1964, doi: 10.1029/2000WR900065.

Tucker, G.E., and Whipple, K.X, 2002, Topographic outcomes predicted by stream erosion models: Sensitivity analysis and intermodel comparison: Journal of Geophysical Research, v. 107, doi: 10.1029/2001JB000162.

Valentine, P.C., Uzmann, J.R., and Cooper, R.A., 1980, Geologic and biologic observations in Oceanographer submarine canyon: Descriptions of dives aboard the research submersibles *Alvin* (1967, 1978) and *Nekton Gamma* (1974): U.S. Geological Survey Open-File Report 80-76, 40 p.

von Huene, R., 1989, Continental margins around the Gulf of Alaska, *in* Winterer, E.L., Hussong, D.M., and Decker, R.W., eds., The eastern Pacific Ocean and Hawaii: Boulder, Colorado, Geological Society of America Decade of North American Geology, v. M, p. 383–401.

von Huene, R., and Kulm, L.D., 1973, Tectonic summary of Leg 18, *in* Kulm, L.D., and von Huene, R., eds., Initial Reports Deep Sea Drilling Project: Washington, D.C., U.S. Government Printing Office, p. 961–976.

Warme, J.E., Slater, R.A., and Cooper, R.A., 1978, Bioerosion in submarine canyons, *in* Stanley, D.J., and Kelling, G., eds., Sedimentation in submarine canyons, fans, and trenches: Stroudsburg, Dowden, Hutchinson and Ross, p. 65–70.

Webber, N.B., 1971, Fluid mechanics for civil engineers: New York, Chapman and Hall, 340 p.

Weissel, J.K., and Seidl, M.A., 1998, Inland propagation of erosional escarpments and river profile evolution across the southeast Australian passive continental margin, *in* Tinkler, K.J., and Wohl, E.E., eds., Rivers over rock: Fluvial processes in bedrock channels: Washington, D.C., American Geophysical Union, p. 189–206.

Wessel, P., and Smith, W.H.F., 1991, Free software helps map and display data: Eos (Transactions, American Geophysical Union), v. 72, p. 441.

Whipple, K.X, and Tucker, G.E., 2002, Implications of sediment-flux-dependent river incision models for landscape evolution: Journal of Geophysical Research, v. 107, p. ETG3-1–ETG3-20, doi: 10.1029/2000JB000044.

Whipple, K.X, Hancock, G.S., and Anderson, R.S., 2000, River incision into bedrock: Mechanics and relative efficacy of plucking, abrasion, and cavitation: Geological Society of America Bulletin, v. 112, p. 490–503, doi: 10.1130/0016-7606(2000)112<0490:RIIBMA>2.3.CO;2.

Wright, L.D., Friedrichs, C.T., Kim, S.C., and Scully, M.E., 2001, Effects of ambient currents and waves on gravity-driven sediment transport on continental shelves: Marine Geology, v. 175, p. 25–45, doi: 10.1016/S0025-3227(01)00140-2.

Xu, J.P., Noble, M.A., and Rosenfeld, L.K., 2004, In-situ measurements of velocity structure within turbidity currents: Geophysical Research Letters, v. 31, L09311, doi: 10.1029/2004GL019718.

Manuscript Received by the Society 6 December 2004
Revised Manuscript Received 22 August 2005
Manuscript Accepted 11 September 2005

Printed in the USA